1993

Active suppression of periodic and transient vibrations of mechanical systems : a study of new and existing approaches

Thomas M. Pratt
San Jose State University

INFORMATION TO USERS

Order Number 1356491

Active suppression of periodic and transient vibrations of mechanical systems: A study of new and existing approaches

Pratt, Thomas M., M.S.

San Jose State University, 1993

ACTIVE SUPPRESSION OF PERIODIC AND TRANSIENT

VIBRATIONS OF MECHANICAL SYSTEMS

A Study of New and Existing Approaches

A Thesis

Presented To

The Faculty of the Department of Mechanical Engineering

San Jose State University

In Partial Fulfillment

of the Requirements for the Degree

Master of Science

by

Thomas M. Pratt
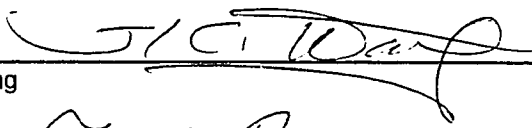
December, 1993
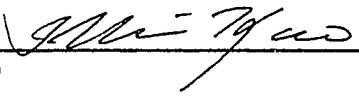
APPROVED FOR THE DEPARTMENT OF MECHANICAL ENGINEERING

_____
Dr. J. C. Wang
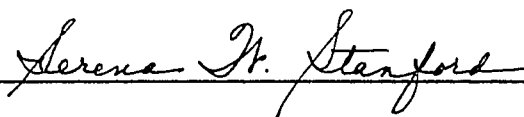
_____
Dr. F. Barez

_____
Dr. I. Kao

APPROVED FOR THE UNIVERSITY

_____

ABSTRACT

ACTIVE SUPPRESSION OF PERIODIC AND TRANSIENT
VIBRATIONS OF MECHANICAL SYSTEMS
A Study of New and Existing Approaches

by Thomas M. Pratt

This thesis presents two methodologies for actively suppressing unwanted mechanical vibrations. The first is an existing computerized algorithm that, when used in conjunction with various measurement and actuating devices, attenuates the vibrations caused by periodic disturbance forces. The second approach uses modern control theory to develop a truly real-time vibration controller. Because of its almost instantaneous processing, this controller cancels both periodic *and* transient vibration signals - a property which is comparatively unique in the realm of mechanical vibration control.

To provide a baseline for comparison, a section illustrating the performance of classical feedback control is also included.

Laboratory testing of the first approach reveals attenuation ranges of 1 to 2 orders of magnitude, which is at least as effective as that predicted for classical feedback control. Computerized simulations of the second approach suggest even better results with the added benefit of a capability for canceling transient vibrations.

ACKNOWLEDGEMENTS

TABLE OF CONTENTS

LIST OF FIGURES

LIST OF FIGURES (CONTINUED)

I.   Introduction

Vibration attenuation has long been an objective of the mechanical engineer, for virtually all me-

chanical devices are subject to some form of unwanted vibration. This attenuation can be ac-

complished by either of two methods: passive vibration mounting, which more or less works by

absorption of the vibration energy, or active vibration control, which attempts to cancel the un-

wanted signal via the addition of an equal and opposite signal. Historically, the passive mount

was the means chosen because the controls technology and electronic and computing resources

needed for adequate active vibration control were limited. The advent of electronic devices such

as the micro-computer and digital signal processor have greatly changed this scenario, however,

and as a result, active systems are becoming increasingly prevalent in vibration control (Inman &

Simonis, 1987; Rogers & Fuller, 1991).

The focus of this project is the investigation of, and comparison between, two types of active con-

trol systems: those that attenuate periodic signals and those which suppress transient signals.

The specific periodic control algorithm utilized in this study functions in the following way: it first

measures the unwanted vibration, then processes the data to create the canceling signal, and

finally introduces the canceling signal back into the system. This control cycle - which will be

shown later to operate via feed-forward control techniques - then repeats indefinitely, thus

achieving permanent vibration attenuation. Clearly, this technology is a vast improvement over

passive mounting, for not only are otherwise "absorbed" vibrations actively canceled, the system

is constantly updating itself to accommodate any changes occurring over time. In fact, the only

significant limitation imposed by such a system is its inability to address signal transients, since

the algorithm does not function on a truly real-time basis. Indeed, it is the attenuation of these

(unpredictable) transients that necessitates the development of an even more adaptive, real-time type of system, an active transient vibration control system.

In an attempt to demonstrate the strengths and weaknesses of both the aforementioned types of systems, this project examines various aspects of each. Since numerous periodic control algorithms have been previously developed, their inclusion in this project is primarily to provide a baseline for the transient type control theory. Specifically, the previously-developed periodic algorithm, Program AVC V3 (Westinghouse Electric Corporation, 1991), is used in a laboratory environment to demonstrate the effectiveness of active control in general. Meanwhile, the development and computerized simulation of a transient type controller is presented to demonstrate the potential for applications requiring more complete vibration attenuation. Finally, the performance of these control methods is compared with that found for uncontrolled and classical-feedback controlled systems. This comparison is accomplished via the computerized simulation and laboratory testing of a simple mechanical system.

II. Mathematical Modeling

As with many academic endeavors, the emphasis for a given piece of work is the demonstration of a generalized theory, rather than a full-scale, real-world application. Consequently, a relatively simple test apparatus was utilized in this project. It is shown below in Figure 1. Referring to the figure, it is desired to minimize the force transmitted to the foundation of the system when the upper mass, m_1, is acted on by a disturbance force, F_d. In order to accomplish this result, the vibration mount supporting the system (represented by k_2 & c_2) must not be subjected to any deflection or motion from above...which implies the intermediate mass, m_2, must be prevented from moving when the disturbance force is acting. This result is to be accomplished using a controller that uses the acceleration of m_1 to predict the motion of m_2; based on this information, it then supplies a voltage to the shaker, m_s, that creates the canceling signal desired.
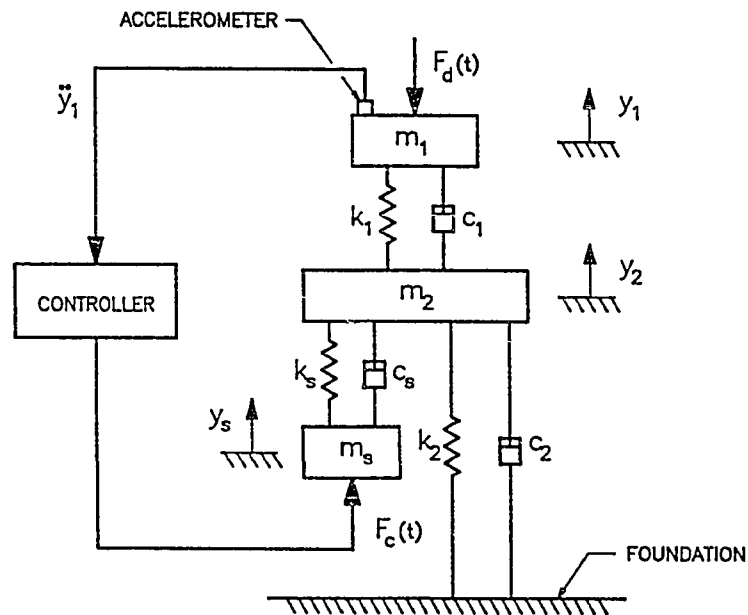
Figure 1: Test Apparatus

This *prediction* of the dynamics of a given body, in this case m_2, is an inherent feature to any feed-forward type of controller. (The more widely known *feedback* type of controller, on the other hand, would operate in a more reactive manner, perpetually lagging the dynamic input). And, as mentioned earlier, both the periodic and transient type controllers addressed in this project utilize this feed-forward control. (The difference, once again, is the means by which they perform this function.) Because of these similarities, the mathematical modeling of the system dynamics is the same for both systems.

III. Open Loop Characteristics

As a basis for the more complex closed-loop models, the open-loop - or free running - nature of the test apparatus must first be understood. Applying Newton' s Second Law, the following differential equations of motion are established:

$$m_1\ddot{y}_1 + c_1(\dot{y}_1 - \dot{y}_2) + k_1(y_1 - y_2) = -F_d(t)$$

$$m_2\ddot{y}_2 - c_1(\dot{y}_1 - \dot{y}_2) + c_s(\dot{y}_2 - \dot{y}_s) + c_2\dot{y}_2 - k_1(y_1 - y_2) + k_s(y_2 - y_s) + k_2y_2 = 0$$

$$m_s\ddot{y}_s - c_s(\dot{y}_2 - \dot{y}_s) - k_s(y_2 - y_s) = F_c(t)$$

where $F_d(t)$ and $F_c(t)$ are treated as separate inputs to the system.

The theoretical physical constants for the system are:

$$m_1 = 1.25\,kg \qquad k_1 = 31,600\,\frac{N}{m} \qquad c_1 = 80\,\frac{N-s}{m}$$

$$m_2 = 1.25\,kg \qquad k_2 = 31,600\,\frac{N}{m} \qquad c_2 = 80\,\frac{N-s}{m}$$

$$m_s = 2.09\,kg \qquad k_s = 74,200\,\frac{N}{m} \qquad c_s = 85\,\frac{N-s}{m}$$

Choosing state variables of:

$$x_1 = y_1 \qquad x_3 = y_2 \qquad x_5 = y_s$$

$$x_2 = \dot{y}_1 \qquad x_4 = \dot{y}_2 \qquad x_6 = \dot{y}_s$$

the following open-loop state-space representation is found:

$$[\dot{x}] \quad = \quad [A] \quad [x] \quad + \quad [B] \begin{bmatrix} F_d \\ \\ F_c \end{bmatrix}$$

$$\begin{bmatrix} \ddot{y}_1 \\ \\ \ddot{y}_2 \end{bmatrix} \quad = \quad [C] \quad [x] \quad + \quad [D] \begin{bmatrix} F_d \\ \\ F_c \end{bmatrix}$$

where:

$$[A] = \begin{bmatrix} 0 & 1 & 0 & 0 & 0 & 0 \\ \dfrac{-k_1}{m_1} & \dfrac{-c_1}{m_1} & \dfrac{k_1}{m_1} & \dfrac{c_1}{m_1} & 0 & 0 \\ 0 & 0 & 0 & 1 & 0 & 0 \\ \dfrac{k_1}{m_2} & \dfrac{c_1}{m_2} & \dfrac{-a}{m_2} & \dfrac{-b}{m_2} & \dfrac{k_s}{m_2} & \dfrac{c_s}{m_2} \\ 0 & 0 & 0 & 0 & 0 & 1 \\ 0 & 0 & \dfrac{k_s}{m_s} & \dfrac{c_s}{m_s} & \dfrac{-k_s}{m_s} & \dfrac{-c_s}{m_s} \end{bmatrix} \qquad [B] = \begin{bmatrix} 0 & 0 \\ \dfrac{-1}{m_1} & 0 \\ 0 & 0 \\ 0 & 0 \\ 0 & 0 \\ 0 & \dfrac{1}{m_s} \end{bmatrix}$$

$$[C] = \begin{bmatrix} \dfrac{-k_1}{m_1} & \dfrac{-c_1}{m_1} & \dfrac{k_1}{m_1} & \dfrac{c_1}{m_1} & 0 & 0 \\ \dfrac{k_1}{m_2} & \dfrac{c_1}{m_2} & \dfrac{-a}{m_2} & \dfrac{-b}{m_2} & \dfrac{k_s}{m_2} & \dfrac{c_s}{m_2} \end{bmatrix} \qquad [D] = \begin{bmatrix} \dfrac{-1}{m_1} & 0 \\ 0 & 0 \end{bmatrix}$$

6

and:

$$a = k_1 + k_2 + k_s$$
$$b = c_1 + c_2 + c_s$$

Using a commercial mathematical simulation software, MATRIX$_x$, the plots on the following pages were generated based on this state-space representation. These plots consist of:

1) Both $\ddot{y}_1$ and $\ddot{y}_2$ versus time for unit step inputs of both F_d and F_c, respectively, as shown in Figure 2. (Initial conditions are all zero.)

and

2) Frequency domain "Bode" plots for both accelerations as caused by each of the input forces as presented in Figures 3 & 4.
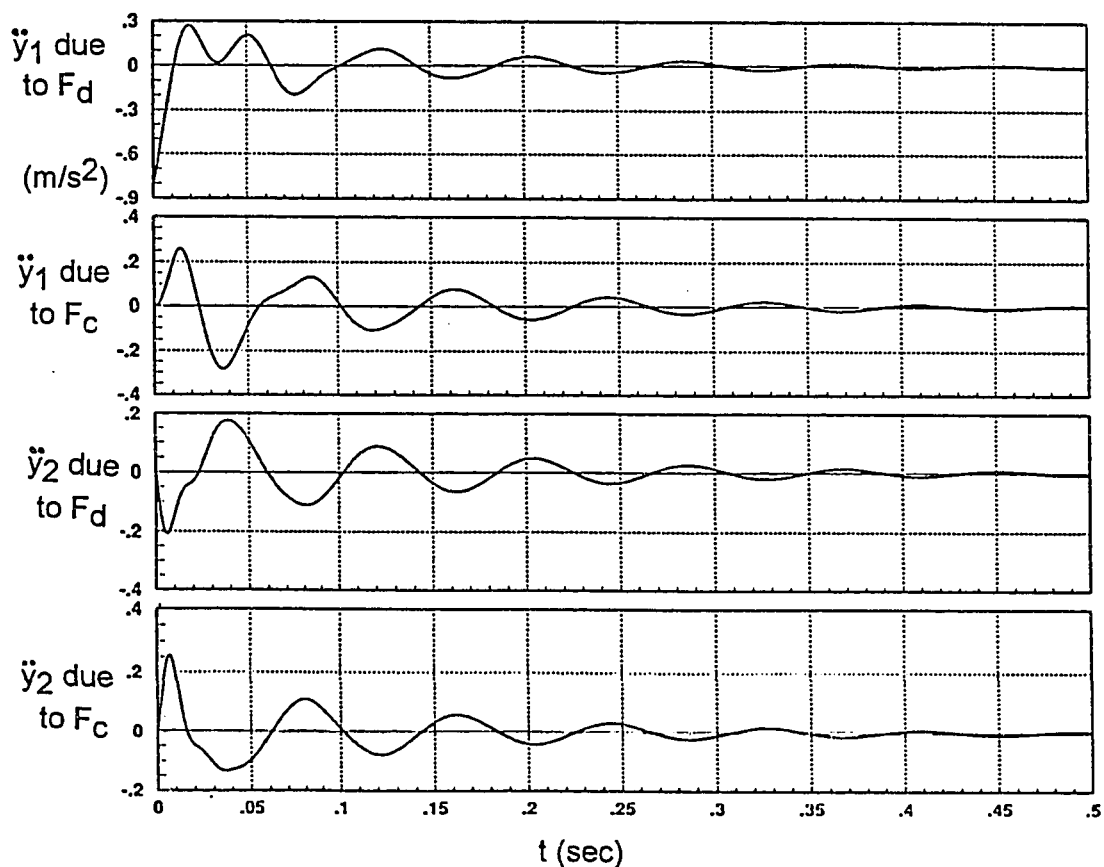
Figure 2: Accelerations vs. Time, Open-Loop System, Step Inputs

7
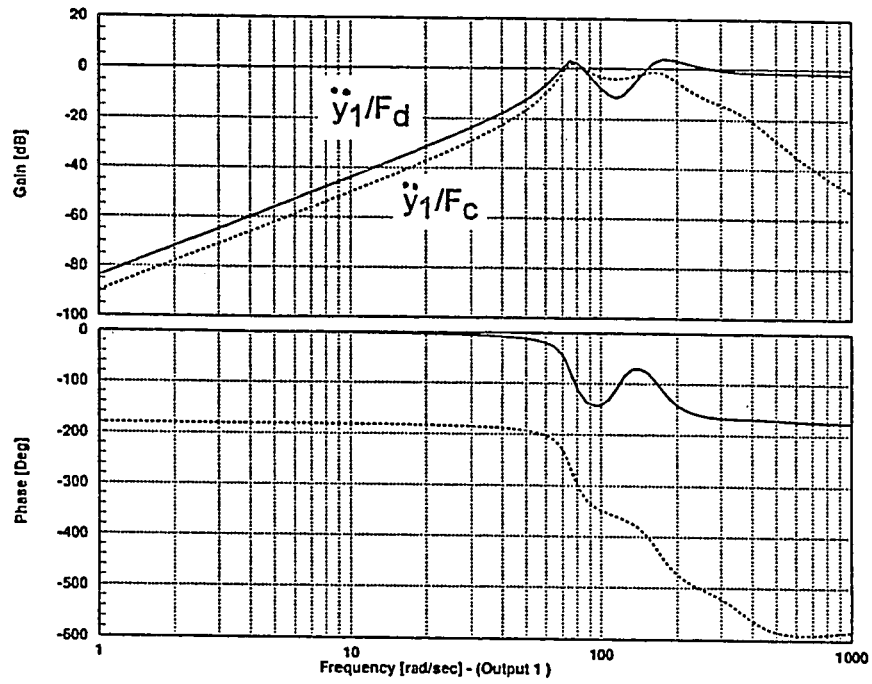
Figure 3: Predicted Frequency Response, $\ddot{y}_1/F_d$ & $\ddot{y}_1/F_c$, Open-Loop System
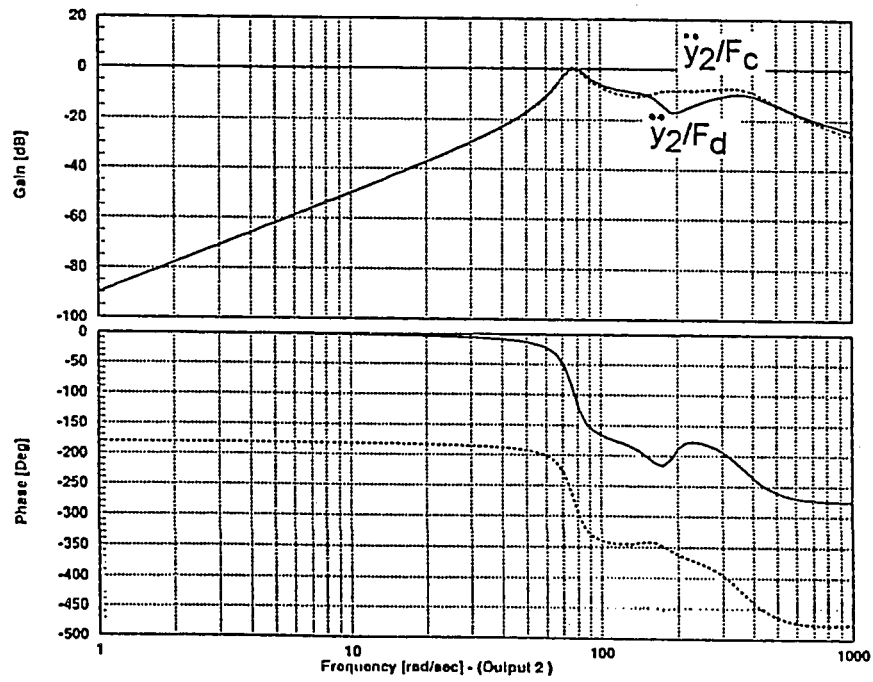
Figure 4: Predicted Frequency Response, $\ddot{y}_2/F_d$ & $\ddot{y}_2/F_c$, Open-Loop System

8

A quick overview of the Bode plots reveals resonant frequencies of approximately 75 Hz and 150 Hz for $\ddot{y}_1$ and a singular resonant frequency for $\ddot{y}_2$ at approximately 75 Hz. The magnitudes of the resonances of $\ddot{y}_1$ are approximately 4 dB, while the magnitude indicated for the $\ddot{y}_2$ resonance is about 0 dB (or unity gain).

In addition to providing insight into the predicted frequency ranges the vibration control algorithms should operate over, the plots discussed above can also be used to validate the accuracy of the dynamic modeling of the system. Using a test apparatus as shown in Figure 5, below, the spring-mass system - which was designed and constructed by San Jose State University undergraduate mechanical engineering students - was oscillated by both the disturbance and control shakers. The responses were then observed and recorded using the Hewlett-Packard 3562A Spectrum Analyzer to produce the experimental Bode plots on the following pages (Figures 6-9).

DISTURBANCE SHAKER

AMPLIFIER

$F_d(t)$

m_1

m_2

m_3

$F_c(t)$

SPECTRUM
ANALYZER

AMPLIFIER
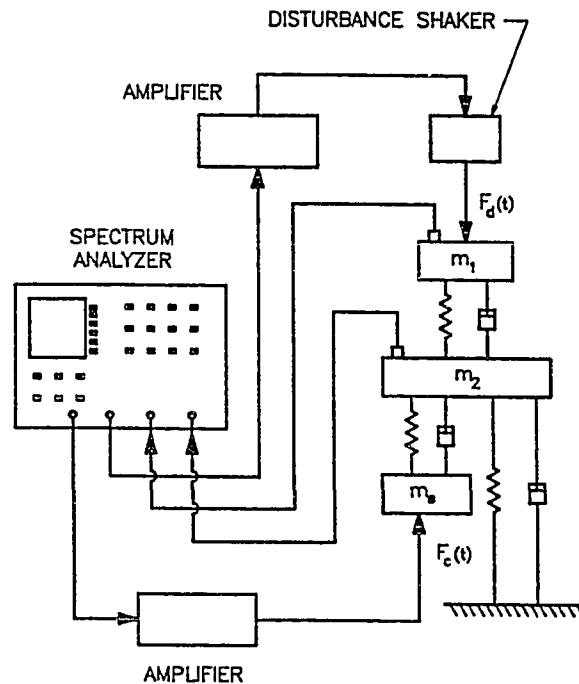
Figure 5: Open-Loop Test Apparatus

Concerning the acceleration of m_1, the graphs for both input forces show some kind of variation in the (otherwise smooth) gain curves at about 75 Hz. This is especially clear on the plot for $\ddot{y}_1$ in response to the control force, F_c (Figure 7): the plot ramps smoothly to a peak of about 6 dB, whereupon it begins to drop appreciably. This response indicates the theoretical model is quite accurate with respect to predicting the resonant frequency and reasonably accurate with respect to the gain. The corresponding phase angle shows a clear change from 0 to -180° over the range where the gain peak occurs, a phenomenon common in classical vibration theory.
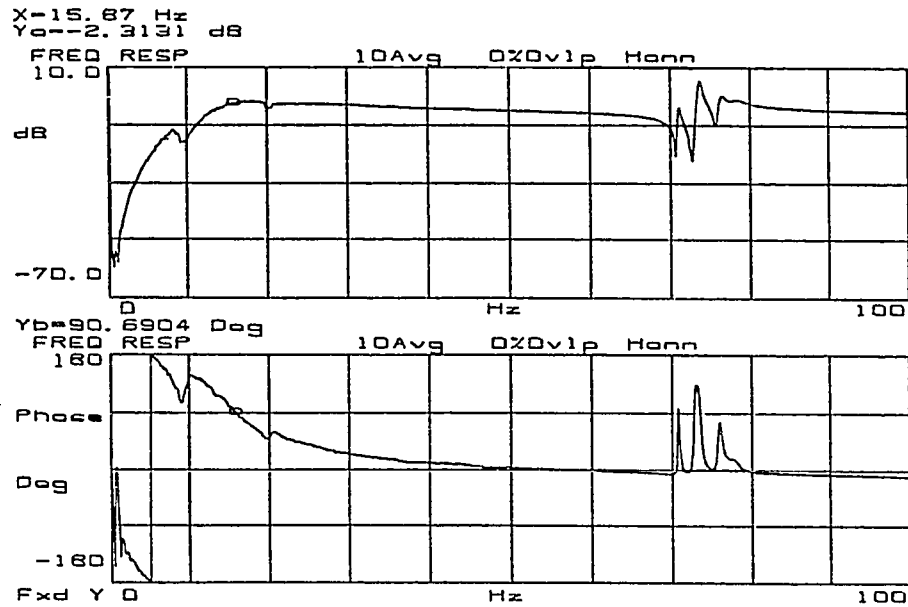
Figure 6: Measured Frequency Response, $\ddot{y}_1/F_d$, Open-Loop System

10

X-20 Hz
Yo--13.723 dB
FREQ RESP   10Avg   0%Ovlp   Hann
12.5

dB

-87.5
         0   Hz   100
Yb=-144.02 Deg
FREQ RESP   10Avg   0%Ovlp   Hann
180

Phase

Deg

-180
Fxd Y 0   Hz   100
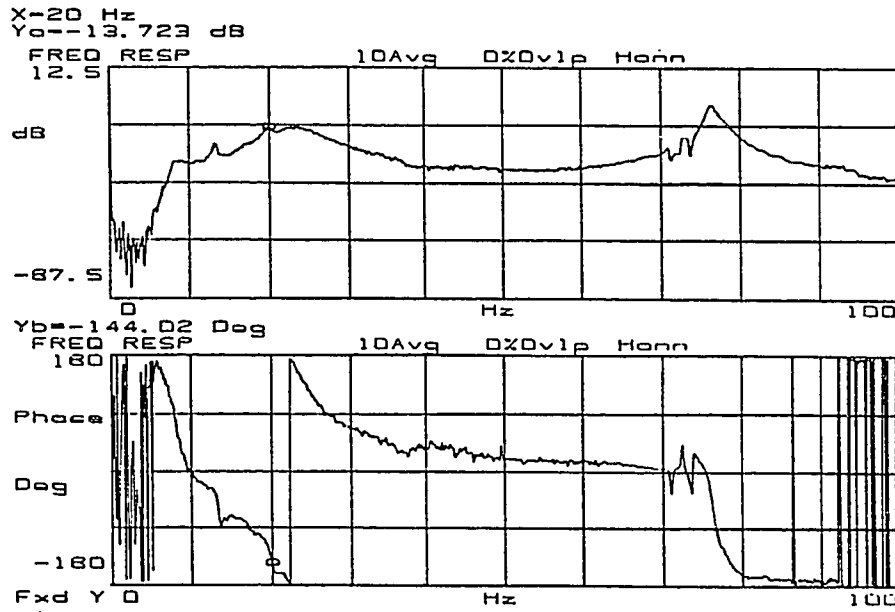
Figure 7: Measured Frequency Response, $\ddot{y}_1/F_c$, Open-Loop System

X-17 Hz
Yo--26.148 dB
FREQ RESP   10Avg   0%Ovlp   Hann
25.0

dB

-75.0
         0   Hz   100
Yb=151.19 Deg
FREQ RESP   10Avg   0%Ovlp   Hann
180

Phase

Deg

-180
Fxd Y 0   Hz   100
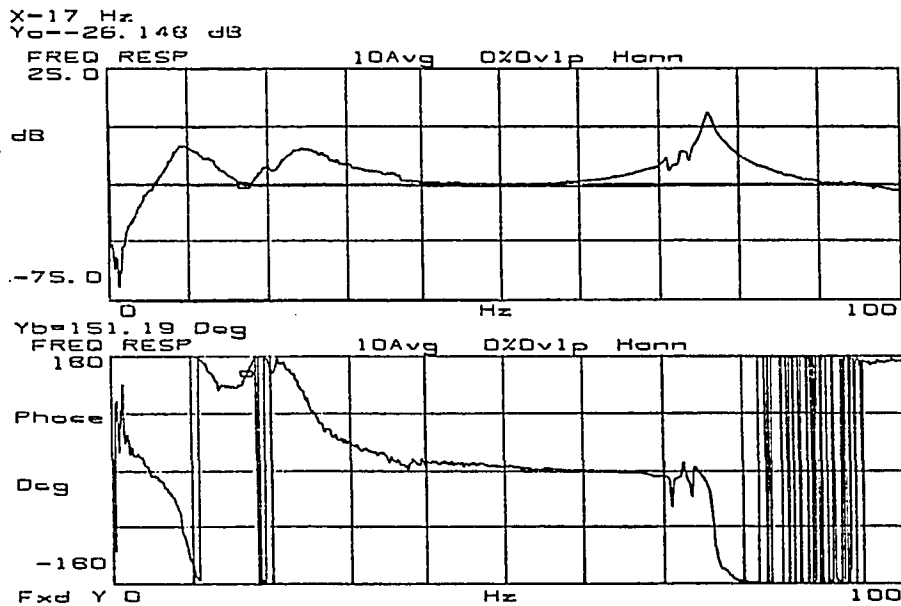
Figure 8: Measured Frequency Response, $\ddot{y}_2/F_d$, Open-Loop System

11

```
Yo--15.654 dB
  FREQ RESP            10Avg    0%Ovlp  Hann
 40.0

  dB


 -120
     0                         Hz            100
Yb=157.635 Dog
  FREQ RESP            10Avg    0%Ovlp  Hann
 180

Phose

 Dog

 -180
Fxd Y  0                       Hz            100
```
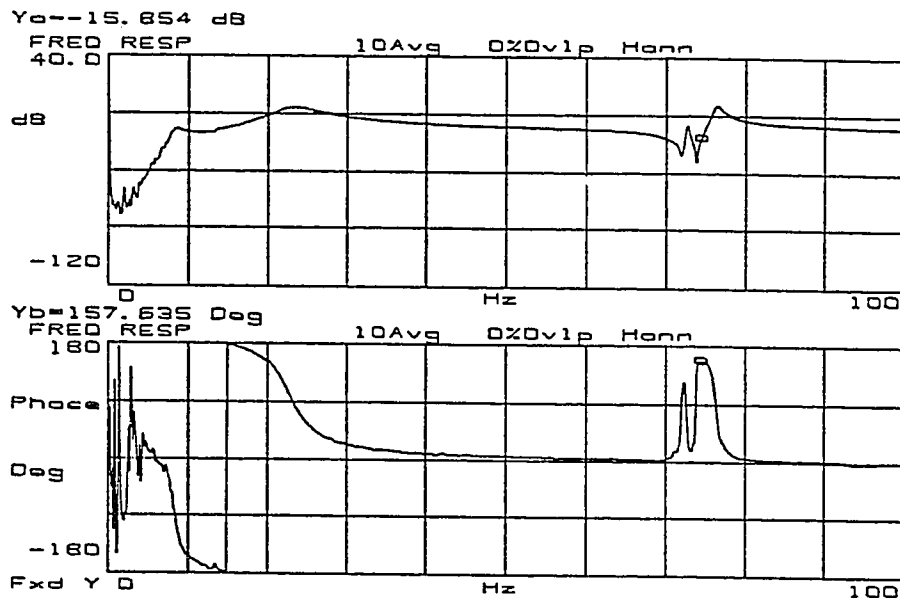
Figure 9: Measured Frequency Response, $\ddot{y}_2/F_c$, Open-Loop System

Unfortunately, the theoretical models for $\ddot{y}_1$ in response to the control force show a

180° phase lag all the way up to the resonant frequency whereupon the angle departs even

further. The explanation for this error is not known, especially since the theoretical and

experimental gain comparison is so close. In contrast, however, the phase relationship for $\ddot{y}_1$ in

response to the disturbance force shows the computer model accurately predicting zero lag up to

the resonant frequency, which is demonstrated by the experimental data. The irony in this

comparison occurs after the resonance: the theoretical model reasonably predicts a change to -

180°, whereas the experimental test shows a continuation of the 0° lag. Further analysis of the

spring-mass system and more laboratory testing is obviously required to determine the cause of

these inaccuracies.

Due to an oversight during this portion of the testing, the analyzer was only programmed to cover

the frequency spectrum up to 100 Hz. Consequently, it is impossible to determine the accuracy

of the theoretical model for $\ddot{y}_1$ with respect to the 150 Hz resonant frequency predicted.

As for the experimental plots of $\ddot{y}_2$ in response to the input forces, the results are again mixed. The best comparison is that for the responses to the disturbance forces: both the theoretical and experimental plots show a resonant frequency at about 75 Hz and both show a 0° phase lag up to the resonant frequency with a phase change to -180° thereafter. The gain is somewhat erroneous, however, inasmuch as the computer model predicted a unity gain at the resonant frequency, while the experimental output showed 6 dB amplification. In comparison, the graphs for $\ddot{y}_2$ in response to the control force - like those for $\ddot{y}_1$ - appear to be significantly off with respect to phase angles, though the gain relationships are close.

Overall, the experimental results appear to corroborate the dynamic behavior of the subject masses predicted by the theoretical models, thus indicating reasonable accuracy of the models. The errors encountered surely demand further investigation to determine whether they resulted from inaccurate modeling or flaws in measurement.

IV. Proportional Feedback Control (for Transient Disturbance Input)

As noted earlier, the nature of both the control algorithms utilized in this project is that they operate via feed-forward characteristics. Because this type of control predicts the response to a given input prior to its occurrence, it tends to be more responsive than classical feedback control. For comparison purposes, however, the spring-mass system used in this project was modeled for control via a simple - and common - feedback control system: a proportional controller.

As shown in Figure 10, the acceleration of m_2 is used as input to the controller. This controller then generates the control force, $F_c(t)$, which is varied in magnitude via the use of a proportional gain, K_p. The control force is then, of course, applied to system to effect the desired vibration cancellation.
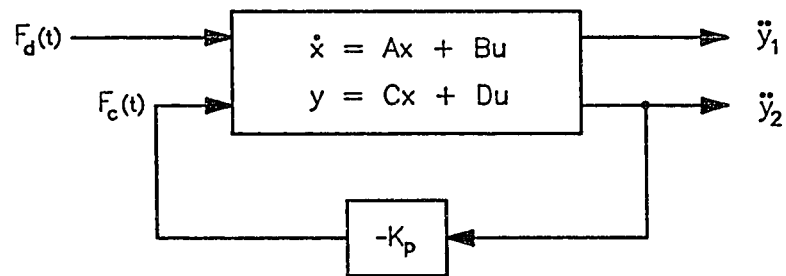
Figure 10: Block Diagram, Proportional Feedback Control

where:

$$F_c = -K_p \ddot{y}_2 = -K_p \dot{x}_4$$

The state-space representation for this control loop is now:

$$
\begin{bmatrix} \dot{x}_1 \\ \dot{x}_2 \\ \dot{x}_3 \\ \dot{x}_4 \\ \dot{x}_5 \\ \dot{x}_6 \end{bmatrix} = \begin{bmatrix} 0 & 1 & 0 & 0 & 0 & 0 \\ \dfrac{-k_1}{m_1} & \dfrac{-c_1}{m_1} & \dfrac{k_1}{m_1} & \dfrac{c_1}{m_1} & 0 & 0 \\ 0 & 0 & 0 & 1 & 0 & 0 \\ \dfrac{k_1}{m_2} & \dfrac{c_1}{m_2} & \dfrac{-a}{m_2} & \dfrac{-b}{m_2} & \dfrac{k_s}{m_2} & \dfrac{c_s}{m_2} \\ 0 & 0 & 0 & 0 & 0 & 1 \\ d & e & f & g & h & n \end{bmatrix} \begin{bmatrix} x_1 \\ x_2 \\ x_3 \\ x_4 \\ x_5 \\ x_6 \end{bmatrix} + \begin{bmatrix} 0 \\ \dfrac{-1}{m_1} \\ 0 \\ 0 \\ 0 \\ 0 \end{bmatrix} [F_d]
$$

where:

$$a = k_1 + k_2 + k_s \qquad\qquad b = c_1 + c_2 + c_s$$

$$d = -K_p\left(\frac{-K_p}{m_2 m_s}\right) \qquad\qquad e = -K_p\left(\frac{c_1}{m_2 m_s}\right)$$

$$f = \frac{k_s}{m_s} + K_p\left(\frac{k_1 + k_2 + k_s}{m_2 m_s}\right) \qquad g = \frac{c_s}{m_s} + K_p\left(\frac{c_1 + c_2 + c_s}{m_2 m_s}\right)$$

$$h = \frac{-k_s}{m_s} - K_p\left(\frac{k_s}{m_2 m_s}\right) \qquad\qquad n = \frac{-c_s}{m_s} - K_p\left(\frac{c_s}{m_2 m_s}\right)$$

The derivation for the equations used above is included in the Appendix B. It should be noted that in contrast to the previously presented open-loop plots, the control force, $F_c(t)$, is now generated implicitly and is no longer an independent input to the system. In other words, the system is now functioning in a closed-loop manner.

15

Using MATRIX$_x$, the following plots (Figures 11-15) were generated for various values of the

feedback gain, K_p, when the system was oscillated by the disturbance input, F_d. Inspection of

the plots reveals attenuation to about 1 order of magnitude (maximum acceleration of

approximately 0.025 g's controlled versus approximately 0.2 g's on the uncontrolled system).

Moreover, the initial large magnitude oscillations are diminished as K_p increases. This behavior

is to be expected with this, or any, negative feedback control system. On the other hand, the

appearance of lower magnitude, steady-state responses is more likely an anomaly of the

modeling software, as all real-world system responses will dampen out when subjected to

transient input. Nonetheless, it is evident that this type of control is effective - over time - in

attenuating the vibration of the subject mass (m_2). As an aside, it should be noted that the

relatively unimpaired magnitude of $\ddot{y}_1$ is completely understandable since the vibration of m_1 is

not the objective.
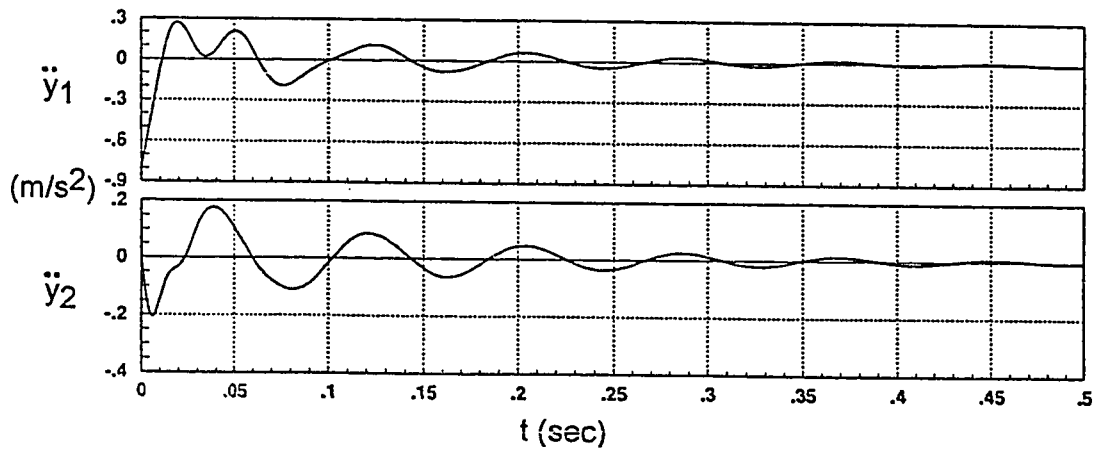
Figure 11: Accelerations ($\ddot{y}_1$ & $\ddot{y}_2$) vs. Time, Proportional Control, K_p=0

16
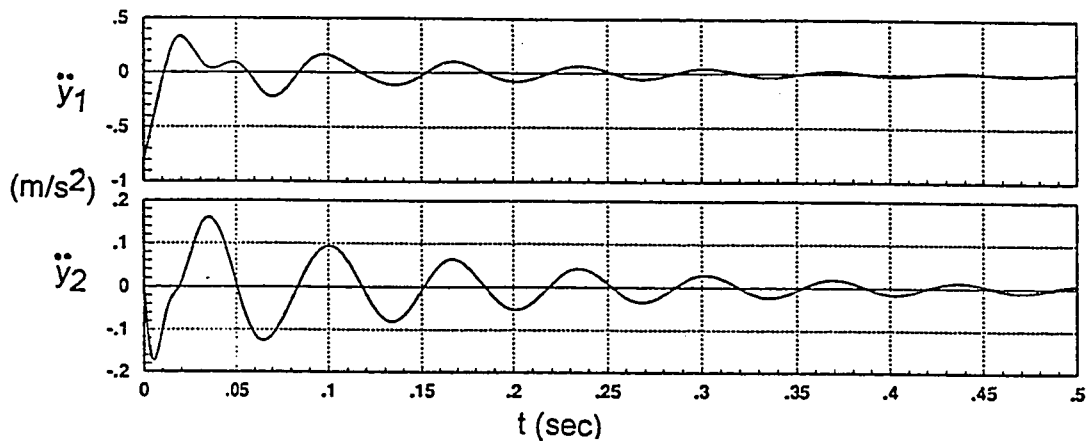
Figure 12: Accelerations ($\ddot{y}_1$ & $\ddot{y}_2$) vs. Time, Proportional Control, $K_p=1$
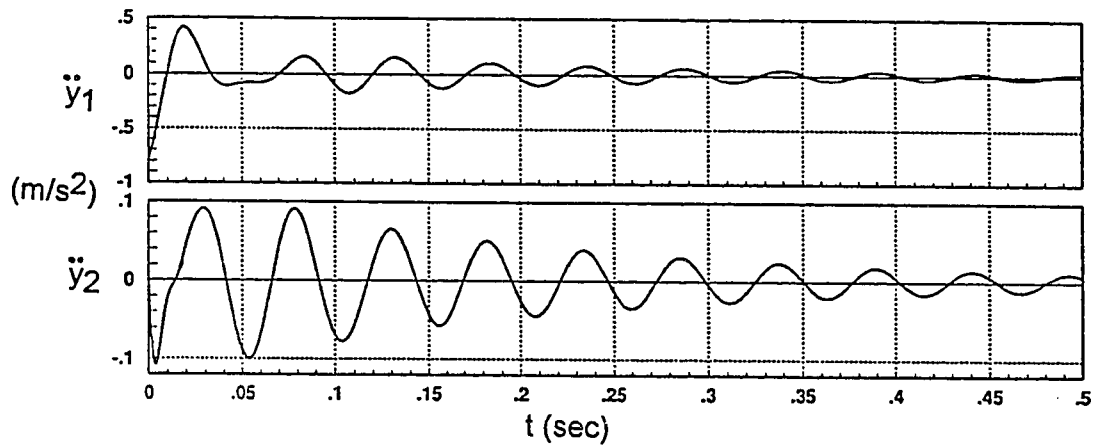
Figure 13: Accelerations ($\ddot{y}_1$ & $\ddot{y}_2$) vs. Time, Proportional Control, $K_p=5$
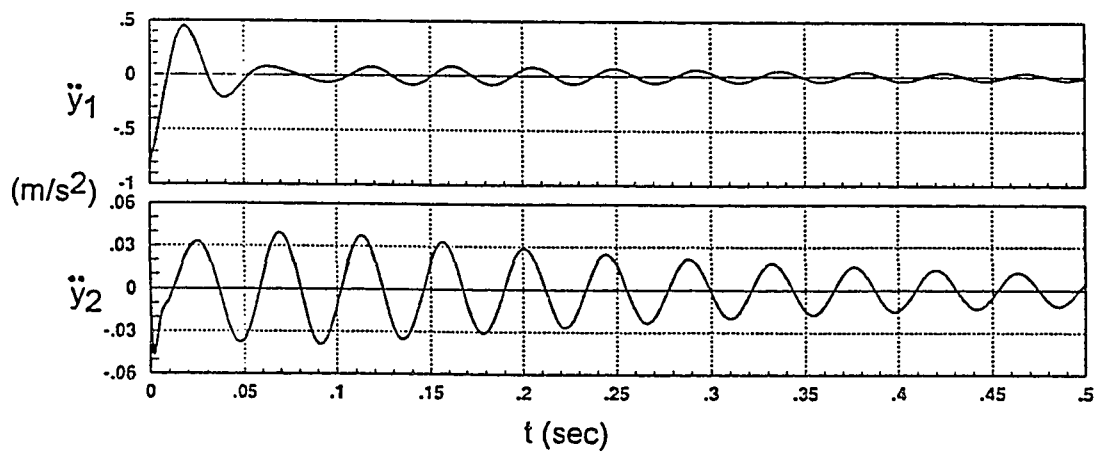
Figure 14: Accelerations ($\ddot{y}_1$ & $\ddot{y}_2$) vs. Time, Proportional Control, $K_p=20$

17
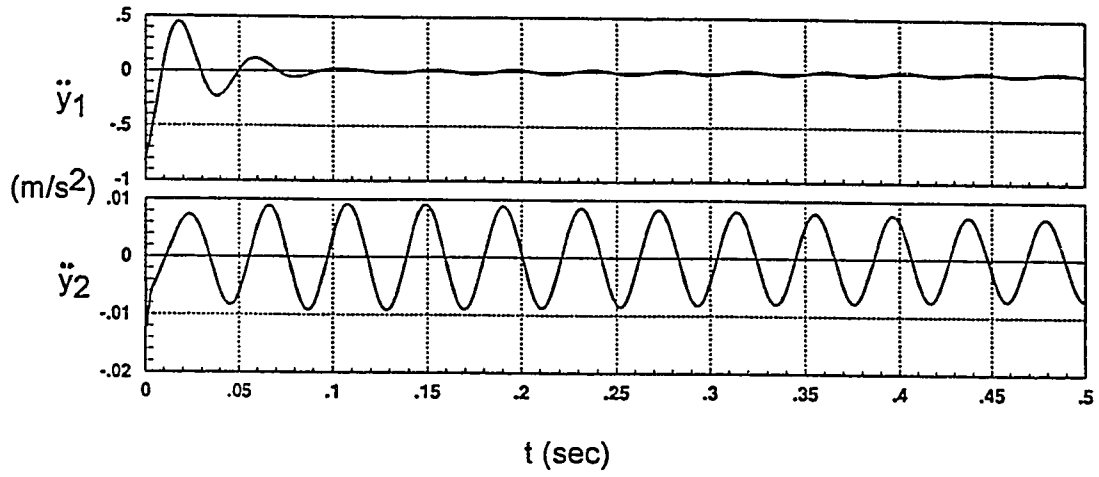
Figure 15: Accelerations ($\ddot{y}_1$ & $\ddot{y}_2$) vs. Time, Proportional Control, K_p=100

V. Active Periodic Control

As alluded to earlier, active feed-forward control is not only an improvement over passive mounts, but is theoretically more responsive (quicker-acting) than classical feedback systems, such as the proportional controller discussed in the previous section. As has also been noted, periodic feed-forward controllers, though comparatively new, are now relatively common (Lukito, 1991; Miller, 1980; Wang, 1990). Because of this, a previously-developed periodic feed-forward controller was used in this project. Unlike the mathematical simulations developed for all the other controllers presented herein, the periodic controller was actually tested on the physical spring-mass apparatus at a Westinghouse Electric Corporation laboratory.

Referring to Figure 16, the configuration and operation of the apparatus was as follows:
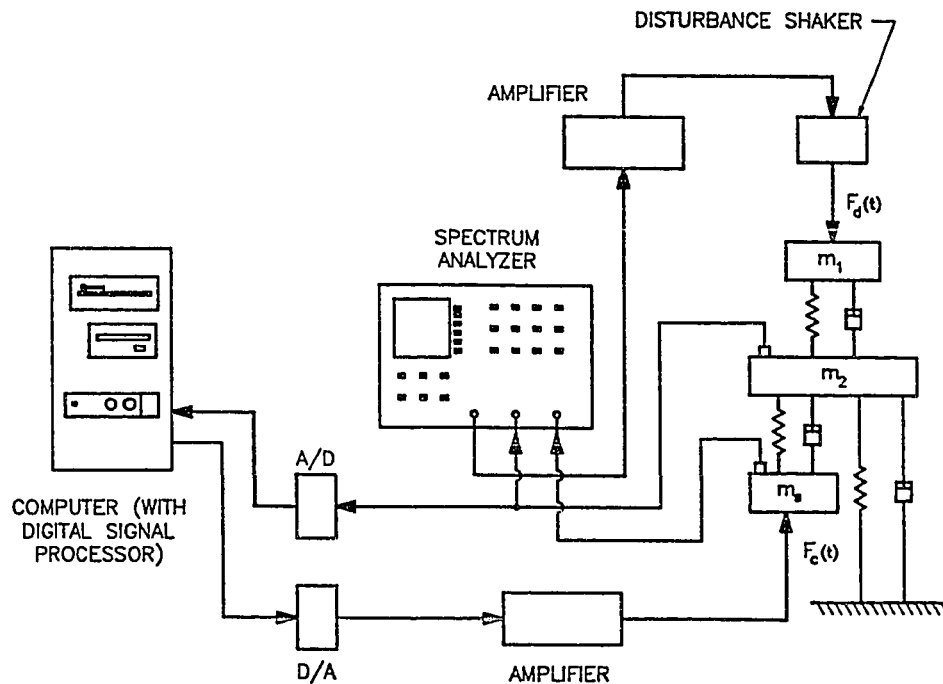
Figure 16: Test Apparatus, Closed-Loop System

1. Prior to operating in a control function, the controller would first generate a known pulse and measure the frequency domain response of the system to this pulse. Using techniques written into the controller software, a frequency response model would then be generated to determine the gain needed at any frequency to suppress the unwanted vibration. (This gain, of course, varies with frequency and is theoretically a maximum at the resonant frequency.)

2. With the system's behavior known, the control function was executed by first initiating a disturbance force, $F_d(t)$, via the shaker mounted to m_1. In the plots presented in the following pages, this disturbance force was always sinusoidal and was generated via the "source" capability of the Hewlett Packard 3562A Spectrum Analyzer (shown in Figure 11).

3. With the system oscillating in response to the disturbance, the acceleration of m_2 was output through the use of the accelerometer mounted to it. This acceleration signal was then fed to an Analog-to-Digital (A/D) converter with a sampling rate 128 times faster than the frequency of the analog signal.

4. Once discretized, the acceleration signal was then processed via the Digital Signal Processor present in the computer. This processing, as mentioned earlier, consisted of:

    a)   The collection of a fixed number of samples (in this case, usually about 2 seconds worth);

    b)   The manipulation of this information, coupled with the anticipated behavior of the system (as determined in step (1)), to create the canceling signal; and

    c)   The output of this canceling signal (in a digital format).

20

The manipulation of the signal was performed using an algorithm, AVC-V3 (Westinghouse Electric Corporation, 1991), that converges on a solution using a mean square error technique. This technique would then effectively generate a filter to cancel the unwanted vibration. Though not developed herein, similar systems are discussed in References 3 and 7.

5. The output of the Digital Signal Processor was transformed back into an analog signal via the Digital-to-Analog (D/A) converter shown in the figure. This signal was then amplified and sent to the electro-mechanical control shaker. Oscillation of the shaker - as effected on the mass of interest, m_2, via the vibration mount represented by k_2 and c_2 - would then (ideally) cancel the vibration caused by the disturbance force.

6. The (hopefully) attenuated vibration of m_2 was then remeasured continuously, thus allowing the controller to constantly update its output to accomodate variations occurring over time.

The sequence noted above is depicted functionally in Figure 17.
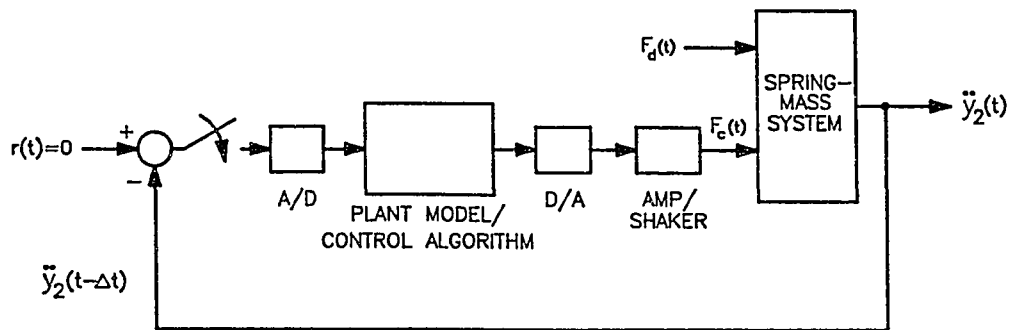
Figure 17: Block Diagram, Active Periodic Control

The measurement of the effectiveness of this controller was accomplished by monitoring the magnitude of the acceleration of m_2 over time as well as the control signal (as measured at the shaker mass). This information was then recorded by the spectrum analyzer and output to an HP plotter. The plots on the following pages (Figures 18-25) depict both of these signals over 10 second windows. It should be noted that the ordinates on the plots are not accelerations *per se*, but voltages directly proportional to accelerations. Since the focus of this analysis is the *relative* reduction of the vibration of mass m_2, rather than the absolute value of its motion, effectiveness of the controller can be accomplished by simple comparison of the voltages associated with the uncontolled vibration versus the controlled one. Moreover, inspection of the plots quickly reveals non-oscillatory behavior. This is because the spectrum analyzer was set up to record the peak values of each oscillation only, which allowed for the maximization of the time window over which signals could be recorded.

The plots on the following pages were obtained for test runs at two different disturbance signal frequencies, 100 Hz and 125 Hz, for which the convergence coefficient, "alpha," on the controller was varied from 0.3 to 0.95. This convergence coeffiecient theoretically correlates to the accuracy of the controller's "model" of the system and its corresponding filtering. A small (0.3) convergence coefficient requires less time to create a canceling signal, but is not quite as accurate as a higher coefficient. The optimum value for this parameter, of course, varies with the application of the control system. Additional analytical insight into the control algorithm and the convergence coefficient can be found in References 7 and 9.
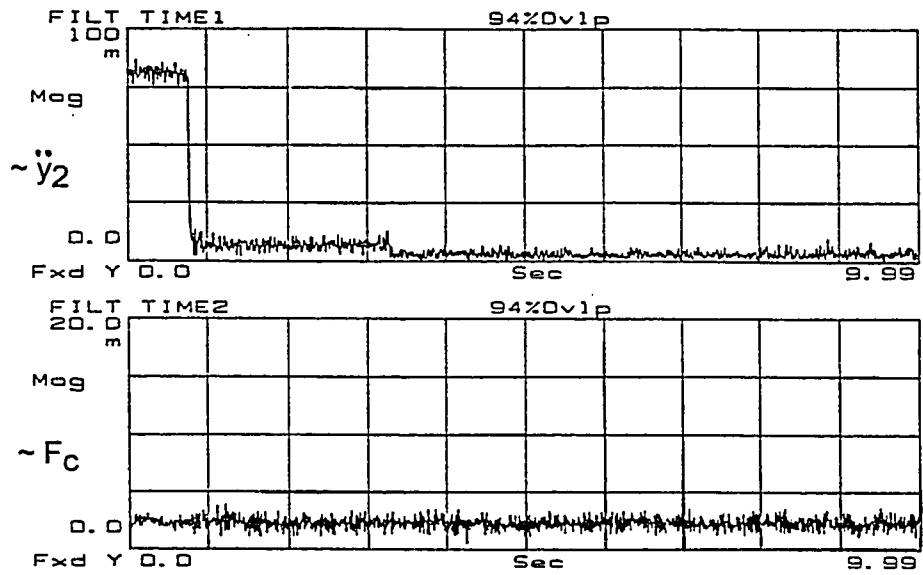
Figure 18: Acceleration & Control Force vs. Time, $f_{disturb}$=100 Hz, alpha=0.30
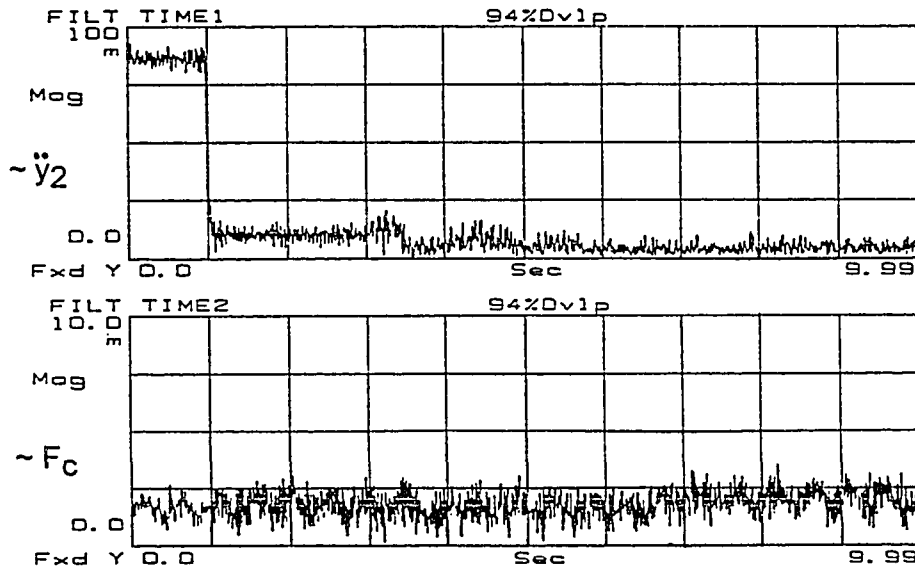
Figure 19: Acceleration & Control Force vs. Time, $f_{disturb}$=100 Hz, alpha=0.50
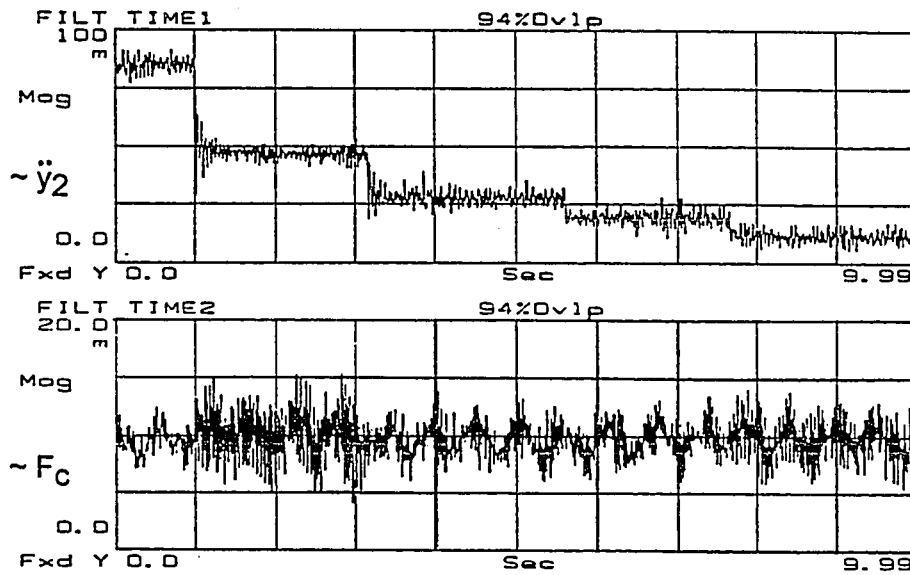
Figure 20: Acceleration & Control Force vs. Time, $f_{disturb}$=100 Hz, alpha=0.80
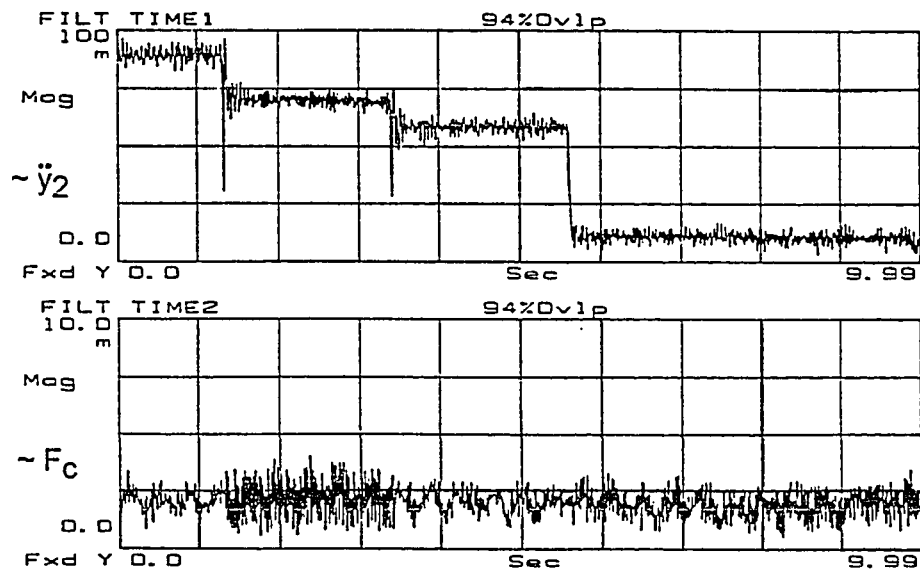
Figure 21: Acceleration & Control Force vs. Time, $f_{disturb}$=100 Hz, alpha=0.95

24
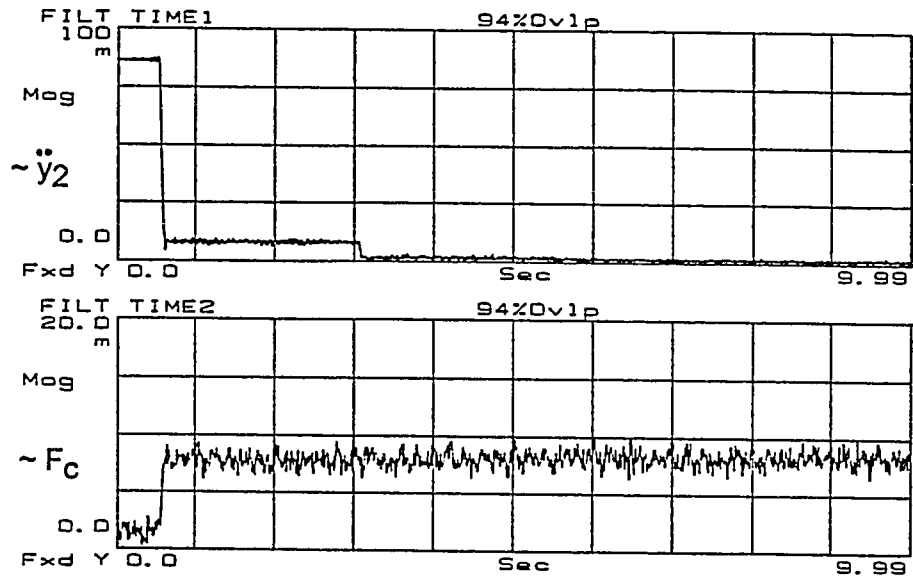
Figure 22: Acceleration & Control Force vs. Time, $f_{disturb}$=125 Hz, alpha=0.30
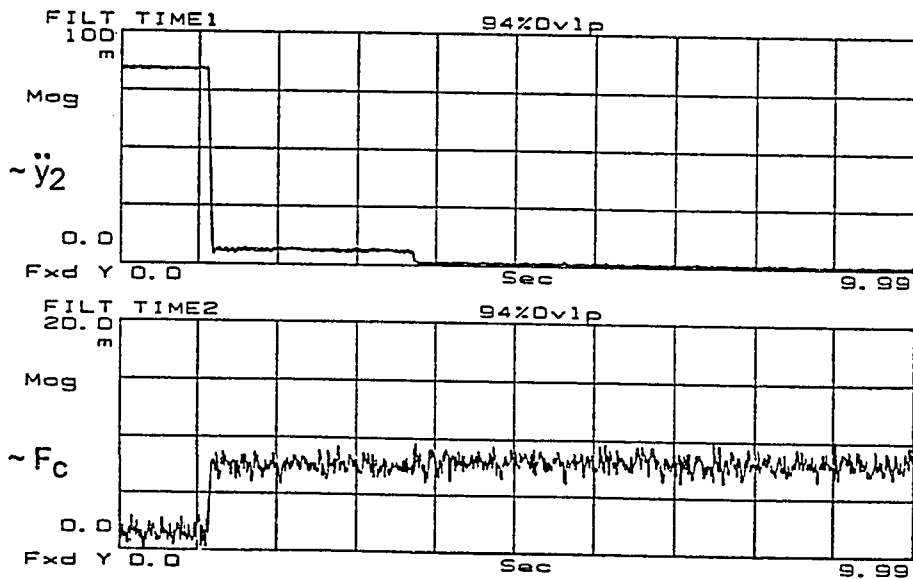
Figure 23: Acceleration & Control Force vs. Time, $f_{disturb}$=125 Hz, alpha=0.50

25
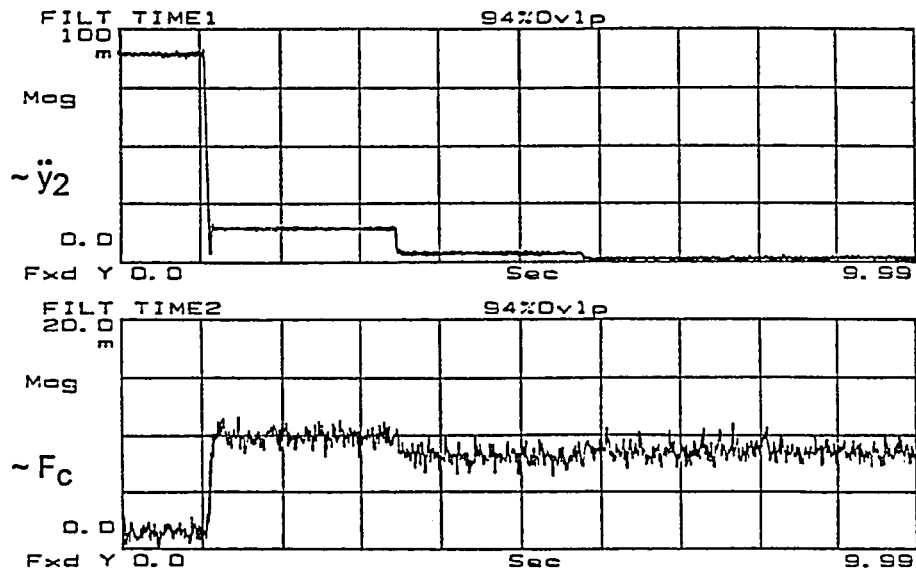
Figure 24: Acceleration & Control Force vs. Time, $f_{disturb}$=125 Hz, alpha=0.80
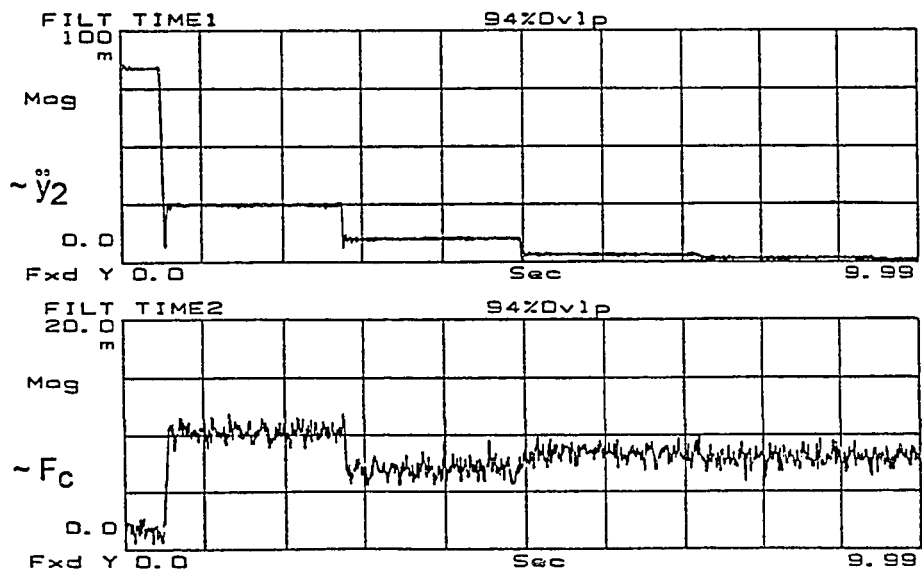
Figure 25: Acceleration & Control Force vs. Time, $f_{disturb}$=125 Hz, alpha=0.95

26

Analysis of the plots shows attenuation ranging from about 1 to 2 orders of magnitude. The worst attenuation found, ironically, is on the plots at 100 Hz with the *higher* convergence coefficients (0.80 & 0.95). These plots show uncontrolled magnitudes of about 85 mV and minimum controlled values on the order of 10-12 mV, thus resulting in an attenuation of 7:1 to 8.5:1 (-17 to -19 dB). This compares roughly equally with the (theoretical) suppresion of the vibration of m_2 using the proportional feedback controller discussed in Section IV.

The best cancellation, on the other hand, is found on all the plots at 125 Hz as well as the plots for the lower convergence coefficients at 100 Hz. These plots show outputs on the order of 2 mV for the same (85-90 mV) inputs. This equates to a reduction of acceleration of as much as 45:1, or -33 dB. This is, without question, a very significant improvement over the proportional controller.

VI. Active Transient Control

The purpose for developing this form of controller, as noted earlier, is to suppress transient vibrations that would not otherwise be controlled by a periodic type controller. As noted in the step-by-step control loop discussion in the previous section, the periodic controller has an initial sampling period during which it is only gathering data and processing it. Consequently, the controller cannot possibly effect any canceling during this time. This means that a transient vibration signal - which may often be just a pulse or other short-lived event - will not be suppressed with this type of controller. Thus, it is the attenuation of these transient vibrations which presents the need for an active transient vibration control system.

As depicted in the block diagram shown in Figure 26, the first attempt at creating the transient feed-forward controller uses the actual disturbance force, $F_d(t)$, as input. (In typical real-world applications, however, it is not known where this force is coming from nor its magnitude.)
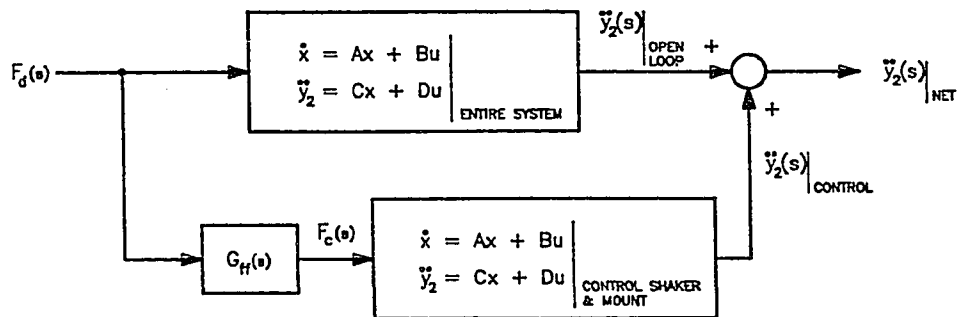
Figure 26: Block Diagram, Idealized Active Transient Control System (uses F_d as controller input)

Using a technique known as Four Pole Parameter Analysis (Snowdon, 1968, 1979), the following transfer function for the spring-mass system was found by Wang (1991) for the relationship between the input disturbance, $F_d(t)$, and the control force, $F_c(t)$:

$$G_{ff}(s) = \frac{F_c(s)}{F_d(s)}$$

$$= -\frac{\left[(m_s c_1)s^3 + (c_1 c_s + k_1 m_s)s^2 + (k_1 c_s + c_1 k_s)s + (k_1 k_s)\right]}{\left[(m_1 c_s)s^3 + (c_1 c_s + k_s m_1)s^2 + (k_s c_1 + c_s k_1)s + (k_1 k_s)\right]}$$

Using this transfer function, the following state-space matrices were established:

$$\begin{bmatrix} \dot{x} \\ \dot{z} \end{bmatrix} = \begin{bmatrix} A & B_c C_{ff} \\ [0]_{3x6} & A_{ff} \end{bmatrix} \begin{bmatrix} x \\ z \end{bmatrix} + \begin{bmatrix} B_d + B_c D_{ff} \\ [0]_{1x1} \end{bmatrix} [F_d]$$

$$\begin{bmatrix} \ddot{y}_{2_{NET}} \end{bmatrix} = \begin{bmatrix} C_{NINE} \end{bmatrix} \begin{bmatrix} x \\ z \end{bmatrix} + [0]_{1x1} \quad [F_d]$$

where:

$$[A] = \begin{bmatrix} \text{Open-loop} \\ \text{System} \\ \text{Dynamics} \\ \text{Matrix} \end{bmatrix} \quad [B_c] = \begin{bmatrix} 0 \\ 0 \\ 0 \\ 0 \\ 0 \\ \dfrac{1}{m_s} \end{bmatrix} \quad [B_d] = \begin{bmatrix} 0 \\ \dfrac{-1}{m_1} \\ 0 \\ 0 \\ 0 \\ 0 \end{bmatrix}$$

29

$$\begin{bmatrix} A_{ff} & B_{ff} \\ \\ C_{ff} & D_{ff} \end{bmatrix} = \quad \begin{matrix} \text{The state-space equivalent of } G_{ff}(s), \text{ numerically evaluated} \\ \\ \text{using MATRIX}_X \end{matrix}$$

$$[C_{NINE}] = \begin{bmatrix} \dfrac{k_1}{m_2} & \dfrac{c_1}{m_2} & \dfrac{-(k_1+k_2+k_s)}{m_2} & \dfrac{-(c_1+c_2+c_s)}{m_2} & \dfrac{k_s}{m_2} & \dfrac{c_s}{m_2} & 0 & 0 & 0 \end{bmatrix}$$

which is the standard output matrix for $\ddot{y}_2$ adjusted to match the other matrix sizes in this model.

Running this system on MATRIX$_X$ generated the plots found on the following pages. As shown in Figures 27-29, the results are very impressive: the attenuation of the response to the step input is approximately 80 dB (or 10,0000:1) as compared to open-loop vibrations. And although the controller is designed to attenuate transient vibrations, it does of course work with steady-state input (as evidenced in Figure 29). Once again, the vibration suppression is in the 4-orders-of-magnitude range.

Figure 27: Frequency Response, $\ddot{y}_2/F_d$, Open-Loop & Idealized Active Transient Control Systems

30
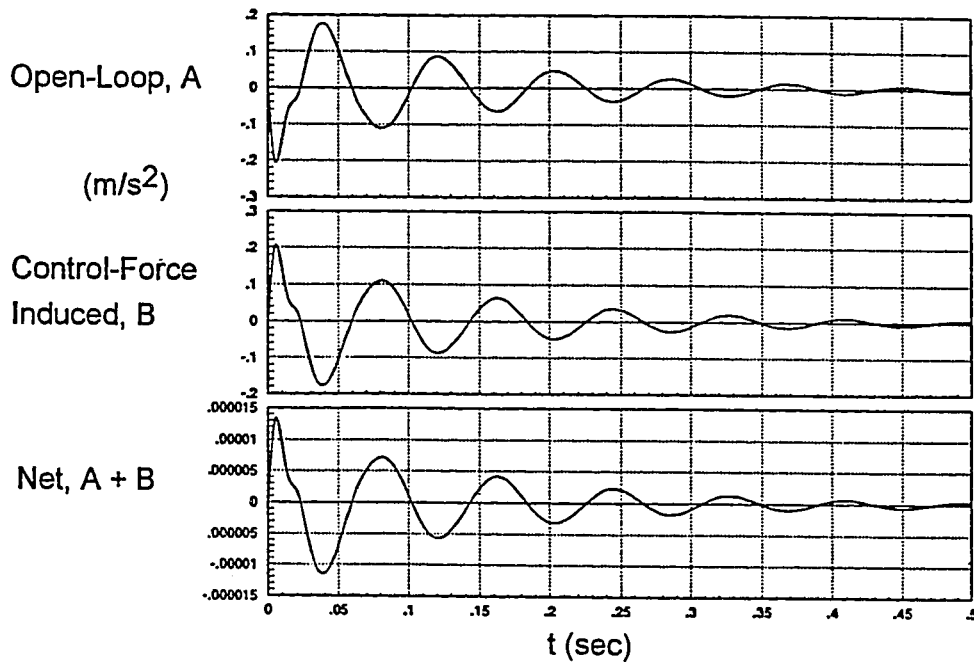
Figure 28: Open-Loop, Control-Force Induced, & Net Accelerations of m_2 vs. Time, Idealized Active Transient Control, Step Disturbance

Figure 29: Open-Loop, Control-Force Induced, & Net Accelerations of m_2 vs. Time, Idealized Active Transient Control, Periodic Disturbance

31

Despite the impressiveness of the previous model, it may be considered only a "textbook" type system since it uses the actual disturbance force to create the control signal. As noted earlier, this information would not typically be known in most real-world situations because the source and magnitude of such a force would not likely be known. The effects of this force, on the other hand, can be measured. In this case, the acceleration of the upper mass, m_1, could be output through the use of an accelerometer mounted to it. Based on this signal, and the proper math model, a similar control force should be theoretically possible.

In order to create the proper math model, the transfer function relating the control force to the acceleration of m_1 must first be created. This transfer function can be derived by either of two methods. The first method is based on the idealized transfer function created in the previous section. Since the overall function relating the control force, $F_c(s)$, to the disturbance force, $F_d(s)$, is already known, the relation of interest can be derived by the following equation:

$$\frac{F_c(s)}{\ddot{y}_1(s)} = \frac{\dfrac{F_c(s)}{F_d(s)}}{\dfrac{\ddot{y}_1(s)}{F_d(s)}}$$

Where the relation between the acceleration of m_1 and $F_d(s)$ is readily found to be:

$$\frac{\ddot{y}_1(s)}{F_d(s)} = \frac{1}{m_1 + \dfrac{c_1}{s} + \dfrac{k_1}{s^2}}$$

This results in the following feed-forward transfer function:

$$\frac{F_c(s)}{\ddot{y}_1(s)} = \frac{as^5 + bs^4 + ds^3 + es^2 + fs + g}{hs^5 + js^4 + ns^3 + ps^2 + qs + r}$$

where:

$$a = m_1 m_s c_1$$

$$f = c_1(k_1 k_s) + k_1(k_1 c_s + c_1 k_s) \qquad n = k_s c_1 + c_s k_1$$

$$b = m_1(c_1 c_s + k_1 m_s) + c_1(m_s c_1)$$

$$g = k_1(k_1 k_s) \qquad p = k_1 k_s$$

$$d = m_1(k_1 c_s + c_1 k_s) + c_1(c_1 c_s + k_1 m_s) + k_1(m_s c_1) \qquad h = m_1 k_s \qquad q = 0$$

$$e = m_1(k_1 k_s) + c_1(k_1 c_s + c_1 k_s) + k_1(c_1 c_s + k_1 m_s) \qquad j = c_1 c_s + k_s m_1 \qquad r = 0$$

Which is equivalent to the following state-space relationship:

$$[\dot{z}] = [A^*] \quad [z] + [B^*] \quad [\ddot{y}_1]$$

$$[F_c] = [C^*] \quad [z] + [D^*] \quad [\ddot{y}_1]$$

where the size of the dynamic matrix, $A^*(s)$, is 5×5 (equivalent to the fifth degree polynomial transfer function relating $F_c(s)$ to $y_1(s)$).

Schematically, this type of control is shown in Figure 30.
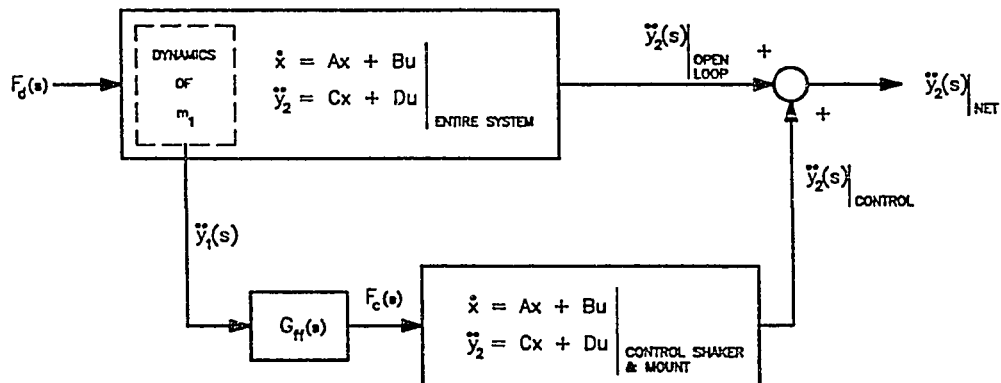
Figure 30: Block Diagram, Practical Active Transient Control System (uses $\ddot{y}_1$ as controller input)

Using these relations and performing some matrix algebra, the following state-space representation was found for this controller:

$$
\begin{bmatrix} \dot{x} \\ \dot{z} \end{bmatrix} = [I-P]^{-1} \begin{bmatrix} A & B_cC^* \\ [0]_{5x6} & A^* \end{bmatrix} \begin{bmatrix} x \\ z \end{bmatrix} + [I-P]^{-1} \quad [B_d] \quad [F_d]
$$

$$
[\ddot{y}_{2_{NET}}] = [C_{ELEVEN}] \begin{bmatrix} x \\ z \end{bmatrix} + [0]_{1x1} \quad [F_d]
$$

where:

$[A] \quad [B_c] \quad [B_d] \quad [A^*] \ \& \ [C^*]$ are previously defined,

$$
[P] = \begin{bmatrix} [0]_{6x1} & B_cD^* & [0]_{6x9} \\ [0]_{5x1} & B^* & [0]_{5x9} \end{bmatrix} \quad ; \text{(derivation appears in Appendix C)}
$$

$[I] = (11 \times 11 \text{ Identity Matrix})$

and

$$
[C_{ELEVEN}] = \begin{bmatrix} \dfrac{k_1}{m_2} & \dfrac{c_1}{m_2} & \dfrac{-(k_1+k_2+k_s)}{m_2} & \dfrac{-(c_1+c_2+c_s)}{m_2} & \dfrac{k_s}{m_2} & \dfrac{c_s}{m_2} & [0]_{5x1} \end{bmatrix}
$$

which is the standard output matrix for $\ddot{y}_2$ adjusted for the size of the current model.

Running a simulation of this model on MATRIX$_x$, the plots shown in Figures 31-33 were established. Analysis of these plots, like those for the idealized system presented in the previous

34

section, shows very effective vibration cancellation. Specifically, the Bode plot shows a peak resonance approximately 60 dB lower than the open-loop system, which is a ratio on the order of 1,000:1. In contrast to the idealized system, this one does not theoretically cancel the vibration as well, but it does represent a system that could operate in a practical application.
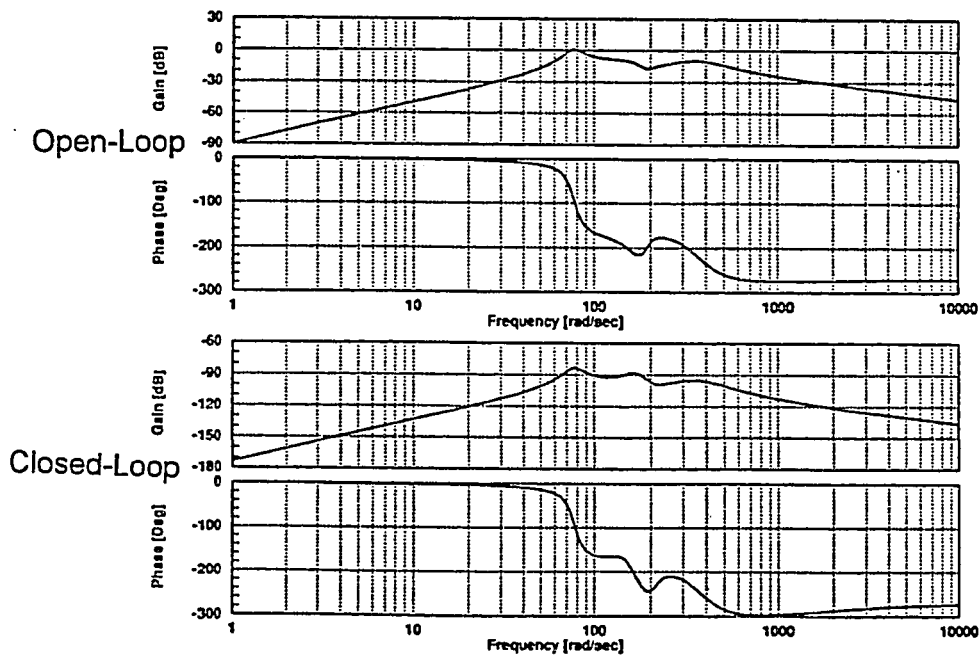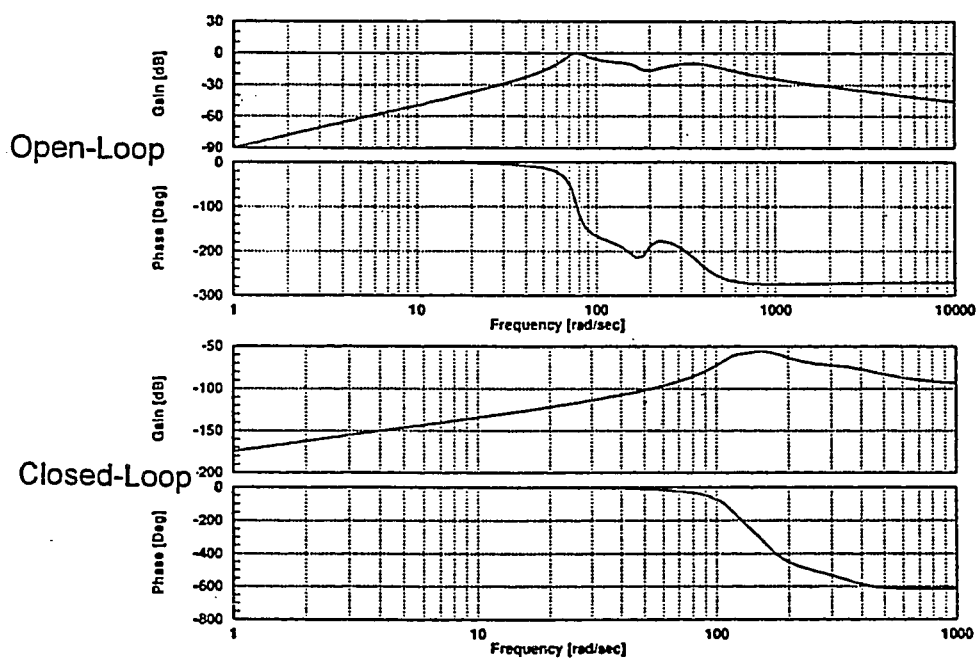

Figure 31: Frequency Response, $\ddot{y}_2/F_d$, Open-Loop & Practical Active Transient Control Systems

Figure 32: Open-Loop, Control-Force Induced, & Net Accelerations of m_2 vs. Time, Practical Active Transient Control, Step Disturbance
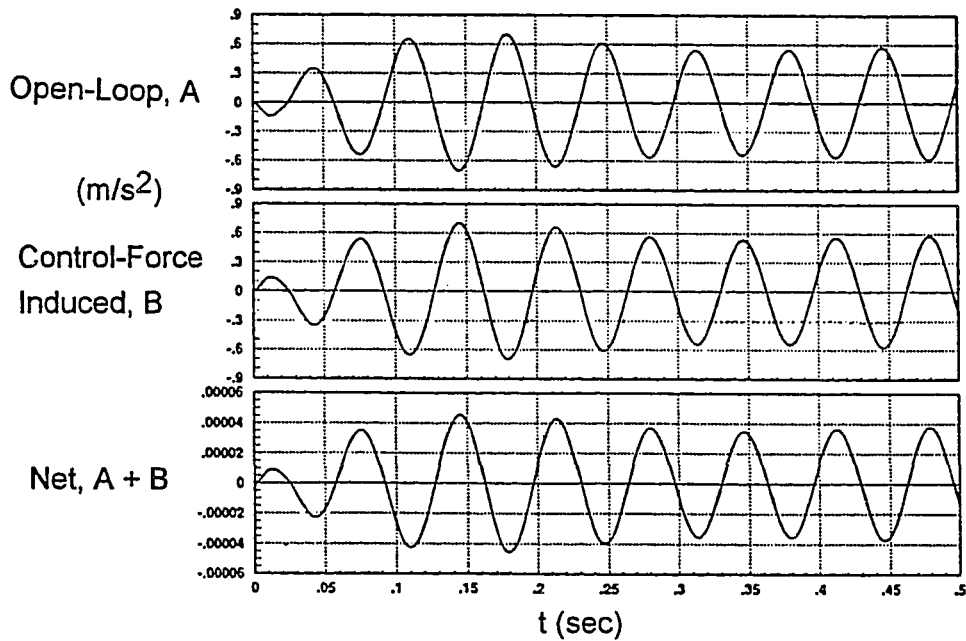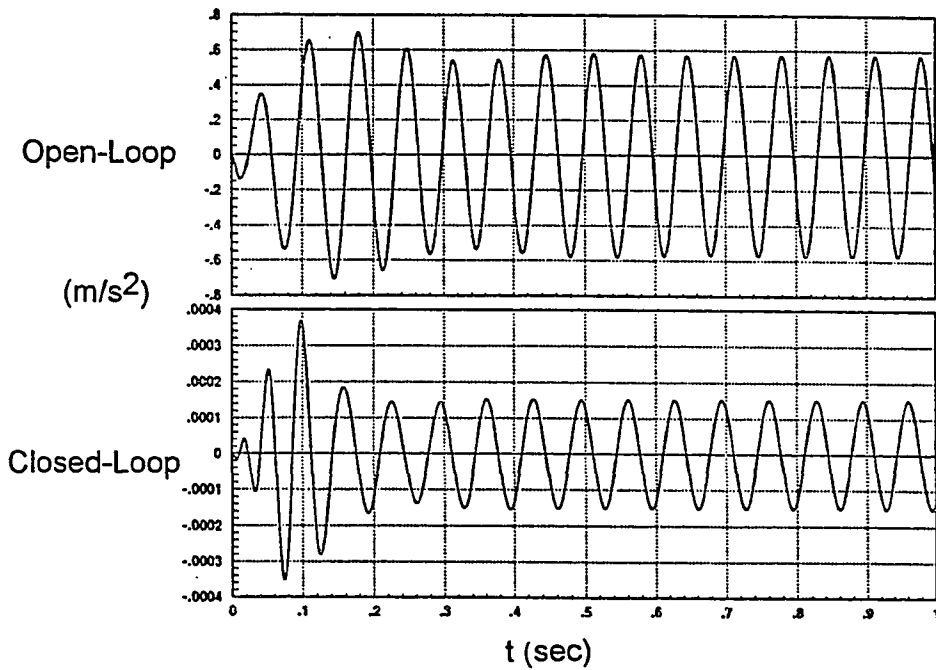

Figure 33: Open-Loop & Net Accelerations of m_2 vs.Time, Practical Active Transient Control, Periodic Disturbance

36

Further inspection of the Bode plot for this model, as well as the time response plot, shows a difference in the characteristics of this system in comparison with the idealized model. First of all, the idealized system oscilllations are roughly at the same frequency as the open-loop (free) responses. In addition, the peak resonance of the Bode plots for these two models occurs at the same frequency and the overall plots have roughly the same gain/phase relationship across the frequency spectrum. The model that uses the acceleration of m_1, on the other hand, shows a much different response: the frequency of oscillation is more than twice as fast as the open-loop system. Moreover, the peak on the Bode plot appears at a much higher frequency (approximately 150 Hz versus 80 Hz) than those on the open-loop plot. These circumstances reflect a change in the eigenvalues of the system when the control is based on the acceleration of m_1. A possible reason for this change might be the fact that the input to the controller on the practical system essentially lags the disturbance input (due to the fact that the mass does not accelerate instantaneously, as the input does, but ramps to a peak acceleration 20 milliseconds later). Essentially, the input on the practical controller ($\ddot{y}_1$) is not as "clean" a signal as the idealized system's input ($F_d(t)$ itself), and the performance of this controller demonstrates this fact.

Regardless of the comparatively less accurate cancellation of the practical system versus the idealized system, as well as the differences in the vibration characteristics, the performance of this controller is, without question, very effective.

As mentioned at the beginning of this section, there is a second way of establishing the transfer function relating $F_c(t)$ to the acceleration of m_1, $\ddot{y}_1(t)$. This method uses the Four Pole Parameter Technique discussed at the beginning of this section and solves for the transfer

function directly (rather than using the division of two transfer functions, as was presented earlier in this section). Application of the Four Pole technique yields the following relation:

$$\frac{F_c(s)}{\ddot{y}_1(s)} = \frac{(m_s c_1)s^3 + (c_1 c_s + k_1 m_s)s^2 + (k_1 c_s + c_1 k_s)s + k_1 k_s}{s^2(c_s s + k_s)}$$

which is equivalent to the following state-space relationship:

$$[\dot{w}] \quad = \quad [A^{**}] \quad [w] \quad + \quad [B^{**}] \quad [\ddot{y}_1]$$

$$[F_c] \quad = \quad [C^{**}] \quad [w] \quad + \quad [D^{**}] \quad [\ddot{y}_1]$$

Once again combining with the open-loop system dynamics and performing some matrix algebra yields:

$$\begin{bmatrix} \dot{x} \\ \\ \dot{w} \end{bmatrix} = [I - P_{NEW}]^{-1} \begin{bmatrix} A & B_c C^{**} \\ \\ [0]_{5 \times 6} & A^{**} \end{bmatrix} \begin{bmatrix} x \\ \\ w \end{bmatrix} + [I - P_{NEW}]^{-1} \quad [B_d] \quad [F_d]$$

$$[\ddot{y}_{2_{NET}}] = [C_{NINE}] \begin{bmatrix} x \\ \\ z \end{bmatrix} + [0]_{1 \times 1} \quad [F_d]$$

where:

$$[A] \qquad [B_c] \qquad [B_d] \qquad [A^{**}] \ \& \ [C^{**}] \quad \text{are previously defined,}$$

38

$$[P_{NEW}] = \begin{bmatrix} [0]_{6\times1} & B_cD^* & [0]_{6\times9} \\ [0]_{5\times1} & B^* & [0]_{5\times9} \end{bmatrix} \quad ; \text{ (derivation appears in Appendix C)}$$

$$[I] = \quad (9 \times 9 \text{ Identity Matrix})$$

and

$$[C_{NINE}] = \begin{bmatrix} \dfrac{k_1}{m_2} & \dfrac{c_1}{m_2} & \dfrac{-(k_1+k_2+k_s)}{m_2} & \dfrac{-(c_1+c_2+c_s)}{m_2} & \dfrac{k_s}{m_2} & \dfrac{c_s}{m_2} & [0]_{3\times1} \end{bmatrix}$$

Based on this model, the plots shown in Figures 34-35 were generated using $MATRIX_X$.
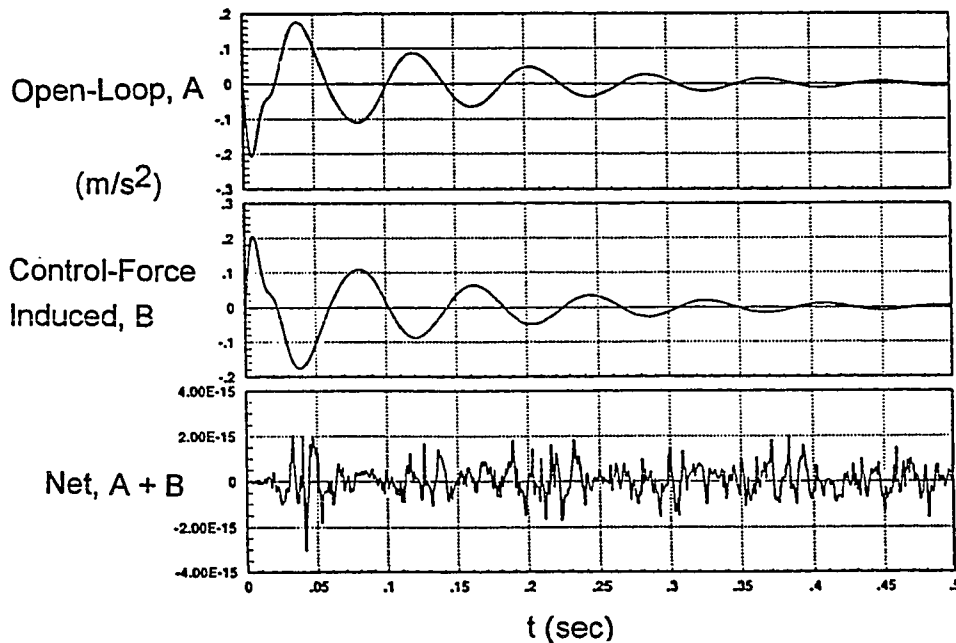
Figure 34: Open-Loop, Control-Force Induced, & Net Accelerations of m_2 vs. Time, Practical Active Transient Control (w/ alternate transfer function $F_c/\ddot{y}_1$), Step Disturbance
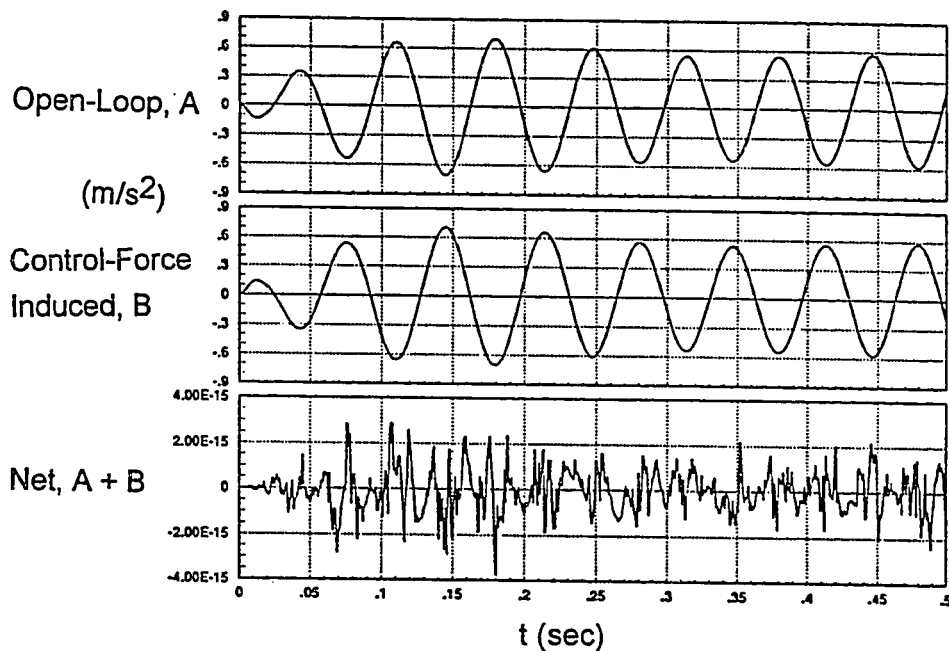
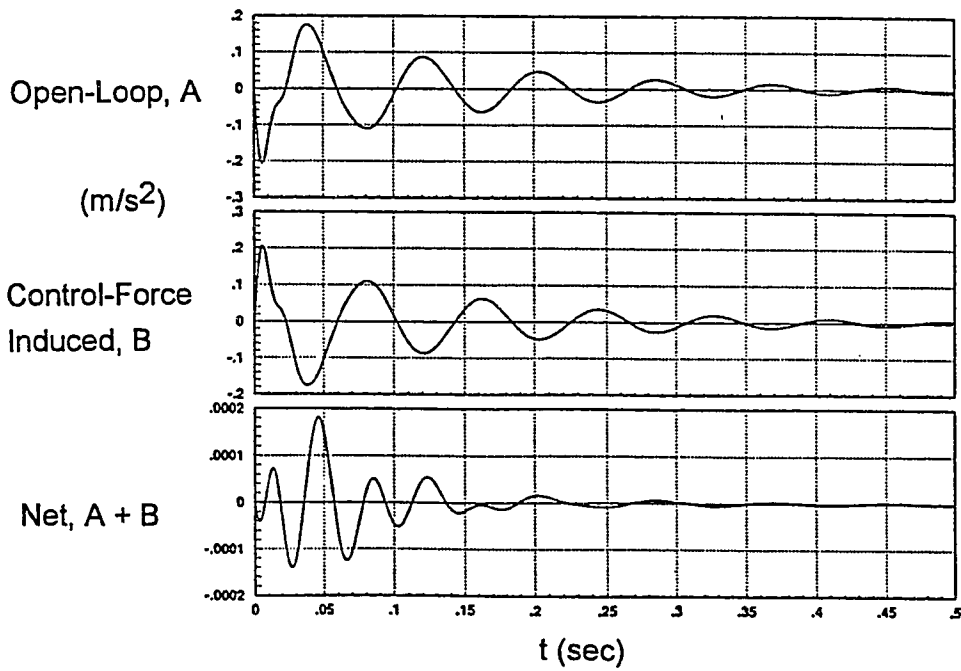**Figure 35:** Open-Loop, Control-Force Induced, & Net Accelerations of m_2 vs. Time, Practical Active Transient Control (w/ alternate transfer function $F_c/\ddot{y}_1$), Periodic Disturbance

Analysis of the output plots for this model once again shows very effective vibration cancellation; in fact, possibly too good. Both the response due to the step disturbance and due to the sinusoidal disturbance show net accelerations of m_2 effectively equal to zero. (Although a Bode plot was not generated for this model, attenuation is on the order of 1 x 10e14:1, or about 280 dB!) Although these results first appear quite encouraging, they do raise some questions.

First off, the best results for attenuation of the vibration of m_2 should occur on the idealized case (because that is the model where the disturbance force itself was used as input to the controller). As noted in the section where that model was presented, the attenuation was found to be about 80 dB. Those results are significantly less accurate than those found with the current model. Secondly, the other model that uses the acceleration of m_1 as input to the controller yielded even less accurate cancellation than the idealized case, which was to be expected. Lastly, the

40

"cleanliness" of the net signal on all the previous models was very smooth and predictable. The outputs on this current model are very noisy and uncertain, which may of course be attributed to numerical round-off error in the control algorithm processing software, but are nonetheless significantly different from the other model outputs.

It is indeed curious as to why the generation of an equivalent, though admittedly simpler, practical transfer function would improve the overall controller performance so well. This is clearly an issue that laboratory testing would quickly resolve. Regardless of the outcome, however, the results yielded by both the practical models (those that use the acceleration of m_1 as controller input) provide a very encouraging basis for further investigation of this type of active control.

VII. Summary of Results

With respect to the various simulations and laboratory tests discussed herein, the following is a summary of results:

1.   The mathematical model and laboratory test data involving the open-loop properties of the spring-mass system are in relative agreement, thus validating the mathematical model. Resonant frequencies of 75 Hz for both m_1 and m_2 (in response to the input forces, F_d & F_c) predicted by the mathematical model were confirmed by the laboratory testing Comparison of the corresponding phase angle relationships, on the other hand, were not quite as accurate.

4.   Computerized simulations of the system when using proportional feedback control reveal vibration attenuation of up to 1 order of magnitude. As feedback gain was increased, overall attenuation improved while (apparent) settling time increased; this observation may be the result of an anomaly in the modeling software.

2.   Active periodic vibration cancellation, using an existing control algorithm in a laboratory environment, shows attenuation of unwanted vibrations ranging from roughly 1 to 2 orders of magnitude (specifically, 17 to 33 dB) when compared to open-loop vibrations. These results are also an improvement - though to a lesser degree - over the cancellation predicted by computer simulations for proportional feedback control The effectiveness of the algorithm varied with respect to both an internal convergence coefficient and the external disturbance frequency.

3.   Computerized simulations of an active transient vibration control system show very effective vibration cancellation, with a minimum attenuation level of 60 dB (about 1,000:1). These results

were found for *both* transient *and* periodic disturbance inputs. Moreover, virtually no perceptible lag time was noticed in these controllers. Results varied with respect to the type of feed-forward transfer function used to generate the control force, F_c.

VIII. Conclusions and Future Work

This project has focused on two types of active vibration suppression methods: an existing one that attenuates periodic vibrations and a new one that cancels both periodic *and* transient vibrations.

Results of laboratory testing of the first type show very effective vibration cancellation. Attenuation of vibrations caused by periodic disturbance forces ranged from as little as 7:1 to as much as 45:1. These results are at least as effective as what would be expected using classical proportional feedback control.

Computerized simulations of mathematical models for the second type of controller are even more impressive. With respect to periodic disturbances, vibration attenuation was found to be no less than 60 dB (about 1,000:1). Provided this degree of vibration suppression can be reproduced in a laboratory environment, it alone would be a significant improvement over the other active control system. Moreover, this approach yielded equally effective cancellation of transient vibrations, a capability that is not even possible with the other controller. Overall, these results provide a very encouraging basis for further studies.

Regarding future work, additional laboratory testing of the existing periodic vibration controller closer to the resonant frequencies of the spring-mass system would provide more insight into its suppression capabilities. As for the new transient vibration controller, development of an algorithm for the digital signal processor would enable laboratory testing to ensue. Such testing would readily determine whether attenuation as effective as that predicted is in fact possible. In addition,

addition, the smaller issue of determining the better of the two feed-forward transfer functions to use in the transient controller could be resolved via such laboratory testing.

References

1. Inman, D. J. & Simonis, J. C. (1987). <u>Vibration Control and Active Vibration Suppression</u> (DE Vol. 4). New York: American Society of Mechanical Engineers.

2. Lukito, H. (1991). <u>Active Vibration Control Methods of Structure Harmonic Vibration Cancellation and Widrow</u>. San Jose: M. S. Report, Mechanical Engineering Dept., San Jose State University.

3. Miller, S. K. (1980). <u>Adaptive Filtering for Active Isolation of Machinery</u>. Cambridge: Massachusetts Institute of Technology - Industry Program on Structure and Acoustics.

4. Rogers, C. A. & Fuller, C. R. (1991). <u>Recent Advances in Active Control of Sound and Vibration</u>. New York: Technomic.

5. Snowdon, J. C. (1968). <u>Vibration and Shock in Damped Mechanical Systems</u>. New York: John Wiley and Sons.

6. Snowdon, J. C. (1979). <u>Vibration Isolation</u>. Washington , DC: U. S. Department of Commerce.

7. Wang, J. C. (1990). <u>Harmonic Vibration Control of Structure</u>. San Jose: Westinghouse Electric Corporation - San Jose State University Technical Report.

8. Westinghouse Electric Corporation (1991). <u>AVC V3</u>. Computer Program. Sunnyvale, CA: Company Private.

9. Widrow, B. & Stearns, S. D. (1985). <u>Adaptive Signal Processing</u>. New York: Prentice Hall, Inc.

Appendix A: Derivation of Open-Loop State-Space Equations

For the system shown below, a system of state-space equations is desired (to facilitate computerized simulations on MATRIX$_X$).
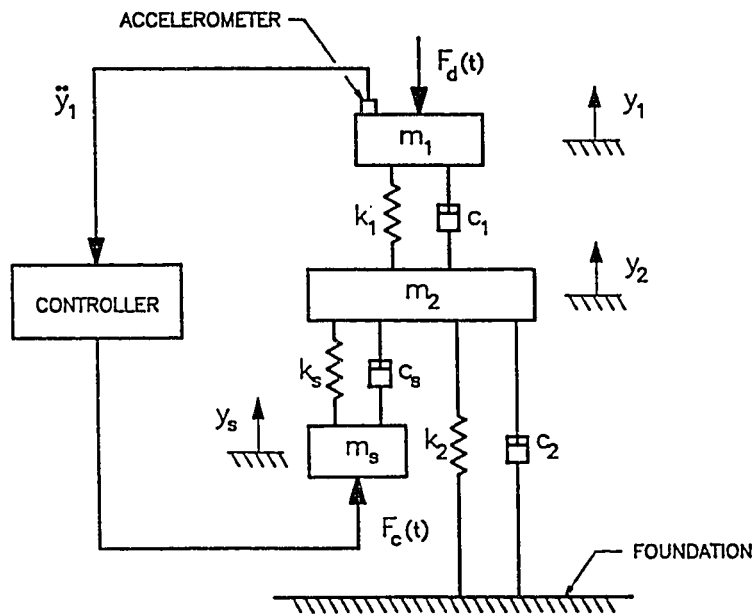
The physical constants for this system are:

$$m_1 = 1.25 \text{kg} \qquad k_1 = 31,600 \frac{N}{m} \qquad c_1 = 80 \frac{N-s}{m}$$

$$m_2 = 1.25 \text{kg} \qquad k_2 = 31,600 \frac{N}{m} \qquad c_2 = 80 \frac{N-s}{m}$$

$$m_s = 2.09 \text{kg} \qquad k_s = 74,200 \frac{N}{m} \qquad c_s = 85 \frac{N-s}{m}$$

Applying Newton's Second Law, the following differential equations of motion are established:

For m_1:

$$\sum F_y = m_1 \ddot{y}_1$$
$$= -F_d - c_1(\dot{y}_1 - \dot{y}_2) - k_1(y_1 - y_2)$$
$$\Rightarrow m_1 \ddot{y}_1 + c_1(\dot{y}_1 - \dot{y}_2) + k_1(y_1 - y_2) = -F_d$$

For m_2:

$$\sum F_y = m_2 \ddot{y}_2$$
$$= k_1(y_1 - y_2) + c_1(\dot{y}_1 - \dot{y}_2) - k_s(y_2 - y_s) - c_s(\dot{y}_2 - \dot{y}_s) - k_2 y_2 - c_2 \dot{y}_2$$
$$\Rightarrow m_2 \ddot{y}_2 - c_1(\dot{y}_1 - \dot{y}_2) + c_s(\dot{y}_2 - \dot{y}_s) + c_2 \dot{y}_2 - k_1(y_1 - y_2) + k_s(y_2 - y_s) + k_2 y_2 = 0$$

and for m_3:

$$\sum F_y = m_s \ddot{y}_s$$
$$= k_s(y_2 - y_s) + c_s(\dot{y}_2 - \dot{y}_s) + F_c$$
$$\Rightarrow m_s \ddot{y}_s - c_s(\dot{y}_2 - \dot{y}_s) - k_s(y_2 - y_s) = F_c$$

Starting with the differential equation for m_1, state variables can now be assigned as:

$$u_1 = F_d \qquad x_3 = y_2$$

$$x_1 = y_1 \qquad x_4 = \dot{x}_3$$

$$x_2 = \dot{x}_1$$

For which the following is found:

$$\dot{x}_2 = \frac{c_1}{m_1}(x_4 - x_2) + \frac{k_1}{m_1}(x_3 - x_1) - \frac{1}{m_1}u_1$$

or:

$$\dot{x}_2 = \frac{-k_1}{m_1}x_1 - \frac{c_1}{m_1}x_2 + \frac{k_1}{m_1}x_3 + \frac{c_1}{m_1}x_4 - \frac{1}{m_1}u_1$$

The equation for m_2 yields:

$$x_5 = y_s \qquad u_2 = F_c$$

$$x_6 = \dot{x}_5$$

For which:

$$\dot{x}_4 = \frac{k_1}{m_2}x_1 + \frac{c_1}{m_2}x_2 + \left[\frac{-k_1}{m_2} - \frac{k_s}{m_2} - \frac{k_2}{m_2}\right]x_3 + \left[\frac{-c_1}{m_2} - \frac{c_s}{m_2} - \frac{c_2}{m_2}\right]x_4 + \frac{k_s}{m_2}x_5 + \frac{c_s}{m_2}x_6$$

and, from the equation for m_3:

$$\dot{x}_6 = \frac{c_s}{m_s}(x_4 - x_6) + \frac{k_s}{m_s}(x_3 - x_5) + \frac{1}{m_s}u_2$$

or

$$\dot{x}_6 = \frac{k_s}{m_s}x_3 + \frac{c_s}{m_s}x_4 - \frac{k_s}{m_s}x_5 - \frac{c_s}{m_s}x_6 + \frac{1}{m_s}u_2$$

3

These relations can now be expressed in matrix form as:

$$
\begin{bmatrix} \dot{x}_1 \\ \dot{x}_2 \\ \dot{x}_3 \\ \dot{x}_4 \\ \dot{x}_5 \\ \dot{x}_6 \end{bmatrix}
=
\begin{bmatrix}
0 & 1 & 0 & 0 & 0 & 0 \\
\dfrac{-k_1}{m_1} & \dfrac{-c_1}{m_1} & \dfrac{k_1}{m_1} & \dfrac{c_1}{m_1} & 0 & 0 \\
0 & 0 & 0 & 1 & 0 & 0 \\
\dfrac{k_1}{m_2} & \dfrac{c_1}{m_2} & a & b & \dfrac{k_s}{m_2} & \dfrac{c_s}{m_2} \\
0 & 0 & 0 & 0 & 0 & 1 \\
0 & 0 & \dfrac{k_s}{m_s} & \dfrac{c_s}{m_s} & \dfrac{-k_s}{m_s} & \dfrac{-c_s}{m_s}
\end{bmatrix}
\begin{bmatrix} x_1 \\ x_2 \\ x_3 \\ x_4 \\ x_5 \\ x_6 \end{bmatrix}
+
\begin{bmatrix}
0 & 0 \\
\dfrac{-1}{m_1} & 0 \\
0 & 0 \\
0 & 0 \\
0 & 0 \\
0 & \dfrac{1}{m_s}
\end{bmatrix}
\begin{bmatrix} u_1 \\ u_2 \end{bmatrix}
$$

where:

$$
a = -\left[\frac{k_1 + k_2 + k_s}{m_2}\right] \qquad b = -\left[\frac{c_1 + c_2 + c_s}{m_2}\right]
$$

The output variables of interest are $\dot{x}_2$ & $\dot{x}_4$, which represent $\ddot{y}_1$ & $\ddot{y}_2$, respectively. The output equations are thus:

$$
\begin{bmatrix} \dot{x}_2 \\ \dot{x}_4 \end{bmatrix}
=
\begin{bmatrix}
\dfrac{-k_1}{m_1} & \dfrac{-c_1}{m_1} & \dfrac{k_1}{m_1} & \dfrac{c_1}{m_1} & 0 & 0 \\
\dfrac{k_1}{m_2} & \dfrac{c_1}{m_2} & \dfrac{-(k_1+k_2+k_s)}{m_2} & \dfrac{-(c_1+c_2+c_s)}{m_2} & \dfrac{k_s}{m_2} & \dfrac{c_s}{m_2}
\end{bmatrix}
\begin{bmatrix} x \end{bmatrix}
+
\begin{bmatrix}
\dfrac{-1}{m_1} & 0 \\
0 & 0
\end{bmatrix}
\begin{bmatrix} u_1 \\ u_2 \end{bmatrix}
$$

This system of equations were simulated for unit step inputs of F_d and F_c on MATRIX$_x$ using the program listing on the following page.

4

'Program for assembling open-loop system matrix for use with MATRIX$_X$'

m1=1.25

m2=1.25

ms=2.09

k1=31600

k2=31600

ks=74200

c1=80

c2=80

cs=85

a=<0 1 0 0 0 0;

    -1*k1/m1 -1*c1/m1 k1/m1 c1/m1 0 0;

    0 0 0 1 0 0;

    k1/m2 c1/m2 -1*(k1+k2+ks)/m2 -1*(c1+c2+cs)/m2 ks/m2 cs/m2;

    0 0 0 0 0 1;

    0 0 ks/ms cs/ms -1*ks/ms -1*cs/ms>

b=<0 0; -1/m1 0; 0 0; 0 0; 0 0; 0 1/ms>

c=<-1*k1/m1 -1*c1/m1 k1/m1 c1/m1 0 0;

    k1/m2 c1/m2 -1*(k1+k2+ks)/m2 -1*(c1+c2+cs)/m2 ks/m2 cs/m2>

d=<-1/m1 0; 0 0>

s=<a b; c d>

5

Appendix B: Derivation of Closed-Loop Proportional Control Relationships

As depicted in the figure below, the spring-mass system is to be modeled using proportional feedback control.
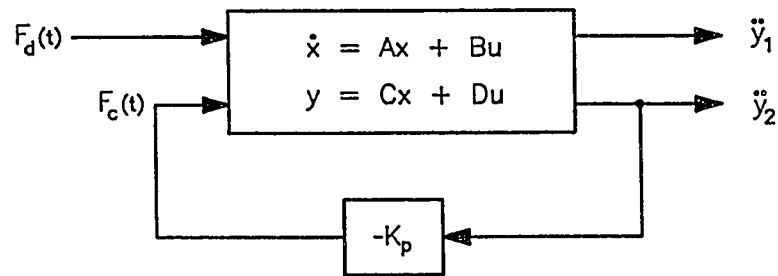
As was shown in Appendix A, the open-loop state-space representation of the spring-mass system is:

$$
\begin{bmatrix} \dot{x}_1 \\ \dot{x}_2 \\ \dot{x}_3 \\ \dot{x}_4 \\ \dot{x}_5 \\ \dot{x}_6 \end{bmatrix}
=
\begin{bmatrix}
0 & 1 & 0 & 0 & 0 & 0 \\
\dfrac{-k_1}{m_1} & \dfrac{-c_1}{m_1} & \dfrac{k_1}{m_1} & \dfrac{c_1}{m_1} & 0 & 0 \\
0 & 0 & 0 & 1 & 0 & 0 \\
\dfrac{k_1}{m_2} & \dfrac{c_1}{m_2} & a & b & \dfrac{k_s}{m_2} & \dfrac{c_s}{m_2} \\
0 & 0 & 0 & 0 & 0 & 1 \\
0 & 0 & \dfrac{k_s}{m_s} & \dfrac{c_s}{m_s} & \dfrac{-k_s}{m_s} & \dfrac{-c_s}{m_s}
\end{bmatrix}
\begin{bmatrix} x_1 \\ x_2 \\ x_3 \\ x_4 \\ x_5 \\ x_6 \end{bmatrix}
+
\begin{bmatrix}
0 & 0 \\
\dfrac{-1}{m_1} & 0 \\
0 & 0 \\
0 & 0 \\
0 & 0 \\
0 & \dfrac{1}{m_s}
\end{bmatrix}
\begin{bmatrix} u_1 \\ u_2 \end{bmatrix}
$$

where:

$$a = -\left[\frac{k_1 + k_2 + k_s}{m_2}\right] \qquad b = -\left[\frac{c_1 + c_2 + c_s}{m_2}\right]$$

This model accounted for the control force, F_c, but only as an independent input (u_2). As the figure on the previous page shows, however, this force is now generated implicitly. It is directly proportional to the acceleration of m_2, or:

$$F_c = -K_p \ddot{y}_2$$

As was also shown in appendix A, $\ddot{y}_2$ is equivalent to the state-space variable $\dot{x}_4$, thus yielding:

$$F_c = -K_p \dot{x}_4$$

Using this relationship, the differential equation for m_s can now be rewritten as:

$$\sum F_y = m_s \ddot{y}_s$$
$$(= m_s \dot{x}_6)$$
$$= k_s(x_3 - x_5) + c_s(x_4 - x_6) - K_p \dot{x}_4$$
$$\Rightarrow \dot{x}_6 = \frac{k_s}{m_s}x_3 + \frac{c_s}{m_s}x_4 - \frac{k_s}{m_s}x_5 - \frac{c_s}{m_s}x_6 - \frac{K_p}{m_s}\dot{x}_4$$

for which the expression for $\dot{x}_4$ is the same as was found in the open-loop model, or:

$$\dot{x}_4 = \frac{k_1}{m_2}x_1 + \frac{c_1}{m_2}x_2 - \frac{(k_1 + k_2 + k_s)}{m_2}x_3 - \frac{(c_1 + c_2 + c_s)}{m_2}x_4 + \frac{k_s}{m_2}x_1 + \frac{c_s}{m_2}x_2$$

Substituting this expression into the one for $\dot{x}_6$ yields:

$$\dot{x}_6 = ax_1 + bx_2 + cx_3 + dx_4 + ex_5 + fx_6$$

where:

$$a = \frac{-K_p k_1}{m_2 m_s} \qquad\qquad b = \frac{-K_p c_1}{m_2 m_s}$$

$$c = \left[\frac{k_s}{m_s} + \frac{K_p(k_1 + k_2 + k_s)}{m_2 m_s}\right] \qquad d = \left[\frac{c_s}{m_s} + \frac{K_p(c_1 + c_2 + c_s)}{m_2 m_s}\right]$$

$$e = \left[\frac{-k_s}{m_s} - \frac{K_p k_s}{m_2 m_s}\right] \qquad\qquad f = \left[\frac{-c_s}{m_s} - \frac{K_p c_s}{m_2 m_s}\right]$$

which yields the following state-space relationship:

$$
\begin{bmatrix} \dot{x}_1 \\ \dot{x}_2 \\ \dot{x}_3 \\ \dot{x}_4 \\ \dot{x}_5 \\ \dot{x}_6 \end{bmatrix}
=
\begin{bmatrix}
0 & 1 & 0 & 0 & 0 & 0 \\
\dfrac{-k_1}{m_1} & \dfrac{-c_1}{m_1} & \dfrac{k_1}{m_1} & \dfrac{c_1}{m_1} & 0 & 0 \\
0 & 0 & 0 & 1 & 0 & 0 \\
\dfrac{k_1}{m_2} & \dfrac{c_1}{m_2} & \dfrac{-(k_1+k_2+k_s)}{m_2} & \dfrac{-(c_1+c_2+c_s)}{m_2} & \dfrac{k_s}{m_2} & \dfrac{c_s}{m_2} \\
0 & 0 & 0 & 0 & 0 & 1 \\
a & b & c & d & e & f
\end{bmatrix}
\begin{bmatrix} x_1 \\ x_2 \\ x_3 \\ x_4 \\ x_5 \\ x_6 \end{bmatrix}
+
\begin{bmatrix} 0 \\ \dfrac{-1}{m_1} \\ 0 \\ 0 \\ 0 \\ 0 \end{bmatrix}
[u_1]
$$

where a, b, c, d, e, & f are defined on the previous page. In addition, since the control force, F_c, is now generated implicitly, the state-space model has only one input, u_1 $(=F_d)$.

The output matrices for this system are:

$$
\begin{bmatrix} \dot{x}_2 \\ \\ \dot{x}_4 \end{bmatrix}
=
\begin{bmatrix}
\dfrac{-k_1}{m_1} & \dfrac{-c_1}{m_1} & \dfrac{k_1}{m_1} & \dfrac{c_1}{m_1} & 0 & 0 & \dfrac{-1}{m_1} \\
\dfrac{k_1}{m_2} & \dfrac{c_1}{m_2} & \dfrac{-(k_1+k_2+k_s)}{m_2} & \dfrac{-(c_1+c_2+c_s)}{m_2} & \dfrac{k_s}{m_2} & \dfrac{c_s}{m_2} & 0
\end{bmatrix}
\; x \; + \; [u_1]
$$

Using the program listing on the following page, the time response plots of $\ddot{y}_1$ & $\ddot{y}_2$ for various values of the feedback gain, K_p, appearing in the main body of this paper were generated using MATRIX$_X$.

4

```
'Program for assembling system matrix for closed-loop proportional control'

print 'input proportional control constant, kp'
inquire kp

m1=1.25
m2=1.25
ms=2.09
k1=31600
k2=31600
ks=74200
c1=80
c2=80
cs=85

a=<0  1  0  0  0  0;
    -1*k1/m1  -1*c1/m1  k1/m1  c1/m1  0  0;
    0  0  0  1  0  0;
    k1/m2  c1/m2  -1*(k1+k2+ks)/m2  -1*(c1+c2+cs)/m2  ks/m2  cs/m2;
    0  0  0  0  0  1;
    0  0  ks/ms  cs/ms  -1*ks/ms  -1*cs/ms>

aa(1,1)=0
aa(5,6)=0
aa(6,1)=-kp*k1/(m2*ms)
aa(6,2)=-kp*c1/(m2*ms)
aa(6,3)=kp*(k1+k2+ks)/(m2*ms)
aa(6,4)=kp*(c1+c2+cs)/(m2*ms)
aa(6,5)=-kp*ks/(m2*ms)
aa(6,6)=-kp*cs/(m2*ms)

atot=a+aa

b=<0;  -1/m1;  0;  0;  0;  0>
```

5

'Program for assembling system matrix for closed-loop proportional control (cont.)'

```
c=<-1*k1/m1  -1*c1/m1  k1/m1  c1/m1  0  0;
    k1/m2  c1/m2  -1*(k1+k2+ks)/m2  -1*(c1+c2+cs)/m2  ks/m2  cs/m2>

d=<-1/m1;  0>

s=<atot  b;  c  d>
```

Appendix C: Derivation of Closed-Loop Active Transient Control Relationships

I.   Control Using F_d as Controller Input:

The block diagram below schematically depicts the approach used to cancel the vibration of m_2 when the system is acted on by the disturbance force, F_d.
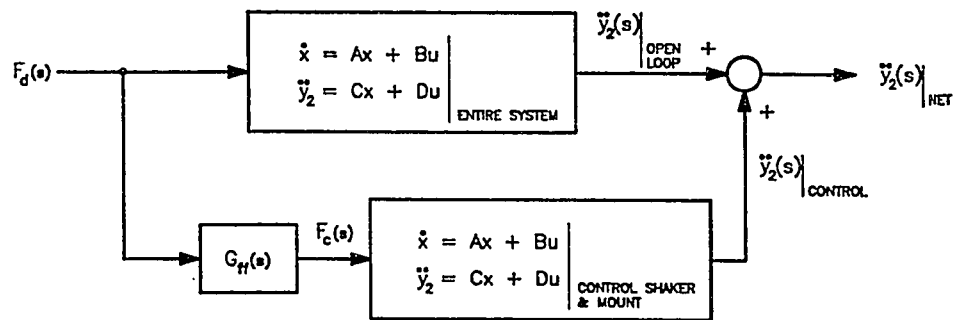
As the diagram shows, the net acceleration of m_2 ($\ddot{y}_2 = \dot{x}_4$) is the sum of the open-loop acceleration and that induced by the controller. Despite this fact, the mass m_2 itself is not acted on by *either* of the external forces directly. (Its motion is affected solely by the vibration mounts adjacent to it.) This fact explains why the expression for $\ddot{y}_{2_{NET}}$, below, does not contain any non-zero contributions from F_d or F_c:

$$[\dot{x}] \quad = \quad [A] \quad [x] \quad + \quad [B_d] \quad [F_d] \quad + \quad [B_c] \quad [F_c]$$

$$[\ddot{y}_{2_{NET}}] \quad = \quad [C] \quad [x] \quad + \quad [0] \quad [F_d] \quad + \quad [0] \quad [F_c]$$

In the this relationship, an expression for the control force (F_c) is required. This expression is the state-space equivalent of the transfer function relating F_c to the disturbance input, F_d. From Wang (1990), the transfer function has been found to be:

$$\frac{F_c(s)}{F_d(s)} = -\left[\frac{(m_s c_1)s^3 + (c_1 c_s + k_1 m_s)s^2 + (k_1 c_s + c_1 k_s)s + k_1 k_s}{(m_1 c_s)s^3 + (c_1 c_s + k_s m_1)s^2 + (k_s c_1 + c_s k_1)s + k_1 k_s}\right]$$

which can be re-written in state-space form as:

$$[\dot{z}] \quad = \quad [A_{ff}] \quad [z] \quad + \quad [B_{ff}] \quad [F_d]$$

$$[F_c] \quad = \quad [C_{ff}] \quad [z] \quad + \quad [D_{ff}] \quad [F_d]$$

where the size of A_{ff} is 3 x 3 (which is equivalent to the third degree polynomial transfer function noted above). The values of the constituent matrices in the system were not evaluated algebraically, but numerically via MATRIX$_x$. For the known values of the physical constants for the system, these matrices were found to be:

$$[A_{ff}] \quad = \quad \begin{bmatrix} -936.9 & -158.5 & -168.4 \\ 512.0 & 0 & 0 \\ 0 & 256.0 & 0 \end{bmatrix} \qquad [B_{ff}] \quad = \quad \begin{bmatrix} 32.0 \\ 0 \\ 0 \end{bmatrix}$$

$$[C_{ff}] \quad = \quad [-24.6 \quad -2.8 \quad -3.0] \qquad [D_{ff}] \quad = \quad [1.6]$$

With the control force, F_c, known, the matrix equations listed at the beginning of this section can be combined and re-written as:

$$\begin{bmatrix} \dot{x} \\ \\ \dot{z} \end{bmatrix} = \begin{bmatrix} A & B_c C_{ff} \\ \\ [0]_{3\times6} & A_{ff} \end{bmatrix} \begin{bmatrix} x \\ \\ z \end{bmatrix} + \begin{bmatrix} B_d + B_c D_{ff} \\ \\ B_{ff} \end{bmatrix} [F_d]$$

2

and

$$
[\ddot{y}_2] = [C_{NINE}] \begin{bmatrix} x \\ \\ \\ z \end{bmatrix} + [0]_{1x1} \quad [F_d]
$$

where:

$$
[A] = \begin{bmatrix} \text{Open} \\ \text{Loop} \\ \text{Dynamics} \\ \text{Matrix} \end{bmatrix} \quad [B_c] = \begin{bmatrix} 0 \\ 0 \\ 0 \\ 0 \\ 0 \\ \dfrac{1}{m_s} \end{bmatrix} \quad [B_d] = \begin{bmatrix} 0 \\ \dfrac{-1}{m_1} \\ 0 \\ 0 \\ 0 \\ 0 \end{bmatrix}
$$

$$
[C_{NINE}] = \begin{bmatrix} \dfrac{k_1}{m_2} & \dfrac{c_1}{m_2} & \dfrac{-a}{m_2} & \dfrac{-b}{m_2} & \dfrac{k_s}{m_2} & \dfrac{c_s}{m_2} & 0 & 0 & 0 \end{bmatrix}
$$

and:

$$
a = k_1 + k_2 + k_s
$$

$$
b = c_1 + c_2 + c_s
$$

and the other matrices were previously defined.

3

Using this model, in the form of the program listing on the following pages, various time-domain and frequency-domain plots were created and are shown in the main body of this paper.

'Program for assembling system matrix for closed-loop transient control using F_d as controller
'input"

m1=1.25
m2=1.25
· ms=2.09
k1=31600
k2=31600
ks=74200
c1=80
c2=80
cs=85

a=<0 1 0 0 0 0;
    -1*k1/m1 -1*c1/m1 k1/m1 c1/m1 0 0;
    0 0 0 1 0 0;
    k1/m2 c1/m2 -1*(k1+k2+ks)/m2 -1*(c1+c2+cs)/m2 ks/m2 cs/m2;
    0 0 0 0 0 1;
    0 0 ks/ms cs/ms -1*ks/ms -1*cs/ms>

num=<167.2 72.84e3 8.62e6 2.34e9>
den=<106.25 99.55e3 8.62e6 2.34e9>

sff=sform(num, den)

aff(1,1)=sff(1,1)   aff(2,1)=sff(2,1)
aff1,2)=sff(1,2)   aff(2,2)=sff(2,2)
aff(1,3)=sff(1,3)   aff(2,3)=sff(2,3)

aff(3,1)=sff(3,1)
aff(3,2)=sff(3,2)
aff(3,3)=sff(3,3)

5

'Program for assembling system matrix for closed-loop transient control using Fd as controller
'input (continued)"

bff(1,1)=sff(1,4)
bff(2,1)=sff(2,4)
bff(3,1)=sff(3,4)

cff(1,1)=sff(4,1)
cff(1,2)=sff(4,2)
cff(1,3)=sff(4,3)

dff(1,1)=sff(4,4)

zero(3,6)=0

acombine=<a bc*cff; zero aff>

bcombine=<bd+bc*dff; bff>

cnine=<k1/m2 c1/m2 -1*(k1+k2+ks)/m2 -1*(c1+c2+cs)/m2 ks/m2 cs/m2 0 0 0>

sff=<acombine bcombine; cnine 0>

II.   Control Using Acceleration of m_1 as Controller Input (First Model)

The system modeled in the previous section was based on a feed-forward controller with an input of the disturbance force, F_d, that acts on the system. As this force is often unknown in most practical vibration control problems, a more useful control system would use a parameter that can be found for this purpose. Since accelerations are readily measured via the use of accelerometers and related electronics, the acceleration of m_1 is used as controller input in this derivation.

In order to create the proper math model, the transfer function relating the control force to the acceleration of m_1 must be created. One method of establishing this transfer function is via the use of the model presented in the previous section. Since the overall function relating the control force, $F_c(s)$, to the disturbance force, $F_d(s)$, is already known, the relation of interest can be found via the following relation:

$$\frac{F_c(s)}{\ddot{y}_1(s)} = \frac{\dfrac{F_c(s)}{F_d(s)}}{\dfrac{\ddot{y}_1(s)}{F_d(s)}}$$

where the relation between the acceleration of m_1 and $F_d(s)$ can be easily determined by the following means:

$$\sum F_y = m_1 \ddot{y}_1$$

$$= k_1 y_1 + c_1 \dot{y}_1 + F_d$$

Taking the Laplace transform of this equation yields:

$$m_1 s^2 Y_1(s) + c_1 s Y_1(s) + k_1 Y_1(s) = -F_d(s)$$

and differentiating twice yields:

$$m_1 \ddot{Y}_1(s) + \frac{c_1}{s} \ddot{Y}_1(s) + \frac{k_1}{s^2} \ddot{Y}_1(s) = -F_d(s)$$

$$\Rightarrow \frac{\ddot{Y}_1(s)}{F_d(s)} = \frac{-1}{m_1 + \dfrac{c_1}{s} + \dfrac{k_1}{s^2}}$$

As was shown in the previous section, the overall transfer function relating F_c to F_d was found to be:

$$\frac{F_c(s)}{F_d(s)} = -\left[\frac{(m_s c_1)s^3 + (c_1 c_s + k_1 m_s)s^2 + (k_1 c_s + c_1 k_s)s + k_1 k_s}{(m_1 c_s)s^3 + (c_1 c_s + k_s m_1)s^2 + (k_s c_1 + c_s k_1)s + k_1 k_s} \right]$$

Therefore, the desired transfer function may now be written as:

$$\frac{F_c(s)}{\ddot{y}_1(s)} = -\frac{\left[\dfrac{(m_s c_1)s^3 + (c_1 c_s + k_1 m_s)s^2 + (k_1 c_s + c_1 k_s)s + k_1 k_s}{(m_1 c_s)s^3 + (c_1 c_s + k_s m_1)s^2 + (k_s c_1 + c_s k_1)s + k_1 k_s} \right]}{\left[\dfrac{1}{m_1 + \dfrac{c_1}{s} + \dfrac{k_1}{s^2}} \right]}$$

8

which is equivalent to:

$$\frac{F_c(s)}{\ddot{y}_1(s)} = \frac{as^5 + bs^4 + ds^3 + es^2 + fs + g}{hs^5 + js^4 + ns^3 + ps^2 + qs + r}$$

where:

$a = m_1 m_s c_1$

$b = m_1(c_1 c_s + k_1 m_s) + c_1(m_s c_1)$

$d = m_1(k_1 c_s + c_1 k_s) + c_1(c_1 c_s + k_1 m_s) + k_1(m_s c_1)$

$e = m_1(k_1 k_s) + c_1(k_1 c_s + c_1 k_s) + k_1(c_1 c_s + k_1 m_s)$

$f = c_1(k_1 k_s) + k_1(k_1 c_s + c_1 k_s)$

$g = k_1(k_1 k_s)$

$h = m_1 c_s$

$j = c_1 c_s + k_s m_1$

$n = k_s c_1 + c_s k_1$

$p = k_1 k_s$

$q = 0$

$r = 0$

This transfer function was then numerically transformed into a state-space system using MATRIX$_X$, yielding:

$$[\dot{z}] \quad = \quad [A^*] \quad [z] \quad + \quad [B^*] \quad [\ddot{y}_1]$$

$$[F_c] \quad = \quad [C^*] \quad [z] \quad + \quad [D^*] \quad [\ddot{y}_1]$$

9

where:

$$[A^*] = \begin{bmatrix} 0 & 0 & 0 & 0 & 0 \\ 0 & 0 & 0 & 0 & 0 \\ 0 & 0 & 0 & 0.0026 & 0 \\ 0 & 0 & 0 & 0 & 0.0051 \\ 0 & 0 & -0.0017 & -0.0016 & -0.0094 \end{bmatrix} \qquad [B^*] = \begin{bmatrix} 0 \\ 0 \\ 0 \\ 0 \\ 5.243 \end{bmatrix}$$

$$[C^*] = \begin{bmatrix} 3.325 & 0.02 & 0 & 0 & 0 \end{bmatrix} \qquad [D^*] = \begin{bmatrix} 0 \end{bmatrix}$$

With this state-space relationship for generation F_C, the overall system model can now be solved. This model has the form:

$$[\dot{x}] = [A] \ [x] + [B_d] \ [F_d] + [B_c] \ [F_c]$$

$$[\ddot{y}_{2_{NET}}] = [C] \ [x] + [0] \ [F_d] + [0] \ [F_c]$$

where:

$$[A] \quad [B_d] \quad [B_c] \quad [C]$$

have been previously defined.

Substituting in the expression derived for F_C (with the physical parameter $\ddot{y}_1$ listed as its state-space variable, $\dot{x}_2$)

10

The overall system now looks like:

$$
\begin{bmatrix} \dot{x} \\ \\ \dot{z} \end{bmatrix} = \begin{bmatrix} A & B_cC^* \\ \\ 0 & A^* \end{bmatrix} \begin{bmatrix} x \\ \\ z \end{bmatrix} + \begin{bmatrix} B_cD^* \\ \\ B^* \end{bmatrix} [\ddot{x}_2] + [B_d] \quad [F_d]
$$

$$
\Rightarrow \begin{bmatrix} \dot{x} \\ \\ \dot{z} \end{bmatrix} - \begin{bmatrix} B_cD^* \\ \\ B^* \end{bmatrix} [\ddot{x}_2] = \begin{bmatrix} A & B_cC^* \\ \\ 0 & A^* \end{bmatrix} \begin{bmatrix} x \\ \\ z \end{bmatrix} + [B_d] \quad [F_d]
$$

Resizing the matrices on the left hand side:

$$
\begin{bmatrix} \dot{x} \\ \\ \dot{z} \end{bmatrix} = [I]_{11 \times 11} \begin{bmatrix} \dot{x} \\ \\ \dot{z} \end{bmatrix}
$$

and:

$$
[P] \equiv \begin{bmatrix} [0]_{6 \times 1} & B_cD^* & [0]_{6 \times 9} \\ \\ [0]_{5 \times 1} & B^* & [0]_{5 \times 9} \end{bmatrix}
$$

yields:

$$
[I-P] \begin{bmatrix} \dot{x} \\ \\ \dot{z} \end{bmatrix} = \begin{bmatrix} A & B_cC^* \\ \\ 0 & A^* \end{bmatrix} \begin{bmatrix} x \\ \\ z \end{bmatrix} + [B_d] \quad [F_d]
$$

11

$$\Rightarrow \begin{bmatrix} \dot{x} \\ \\ \dot{z} \end{bmatrix} = [I-P]^{-1} \begin{bmatrix} A & B_cC^* \\ \\ [0]_{5x6} & A^* \end{bmatrix} \begin{bmatrix} x \\ \\ z \end{bmatrix} + [I-P]^{-1} \quad [B_d] \quad [F_d]$$

and the output matrix is

$$[C_{ELEVEN}]_{1x11} = \begin{bmatrix} C & [0]_{1x5} \end{bmatrix}$$

where $[C]$ has been previously defined.

Using this model, in the form of the program listing on the following page, various time-domain and frequency-domain plots were created and are shown in the main body of this paper.

12

'Program for assembling system matrix for closed-loop transient control using $\ddot{y}_1$ as controller
'input (first model)"

```
m1=1.25
m2=1.25
ms=2.09
k1=31600
k2=31600
ks=74200
c1=80
c2=80
cs=85


a=<0  1  0  0  0  0;
    -1*k1/m1  -1*c1/m1  k1/m1  c1/m1  0  0;
    0  0  0  1  0  0;
    k1/m2  c1/m2  -1*(k1+k2+ks)/m2  -1*(c1+c2+cs)/m2  ks/m2  cs/m2;
    0  0  0  0  0  1;
    0  0  ks/ms  cs/ms  -1*ks/ms  -1*cs/ms>

bb=<0;  -1/m1;  0;  0;  0;  0>

cc=<k1/m2  c1/m2  -1*(k1+k2+ks)/m2  -1*(c1+c2+cs)/m2  ks/m2  cs/m2>

dd=<0>

num=<-2.09e2  -1.044e5  -2.189e7  -5.923e9  -4.6e11  -7.4093e13>
den=<1.063e2  9.955e4  8.622e6  2.345e9  0  0>

sstar=sform(num, den)
```

'Program for assembling system matrix for closed-loop transient control using $\ddot{y}_1$ as controller
'input, first model (continued)"

```
astar(1,1)=sstar(1,1)              astar(2,1)=sstar(2,1)
astar(1,2)=sstar(1,2)              astar(2,2)=sstar(2,2)
astar(1,3)=sstar(1,3)              astar(2,3)=sstar(2,3)
astar(1,4)=sstar(1,4)              astar(2,4)=sstar(2,4)
astar(1,5)=sstar(1,5)              astar(2,5)=sstar(2,5)


astar(3,1)=sstar(3,1)              astar(4,1)=sstar(4,1)
astar(3,2)=sstar(3,2)              astar(4,2)=sstar(4,2)
astar(3,3)=sstar(3,3)              astar(4,3)=sstar(4,3)
astar(3,4)=sstar(3,4)              astar(4,4)=sstar(4,4)
astar(3,5)=sstar(3,5)              astar(4,5)=sstar(4,5)


astar(5,1)=sstar(5,1)
astar(5,2)=sstar(5,2)
astar(5,3)=sstar(5,3)
astar(5,4)=sstar(5,4)
astar(5,5)=sstar(5,5)


bstar(1,1)=sstar(1,6)
bstar(2,1)=sstar(2,6)
bstar(3,1)=sstar(3,6)
bstar(4,1)=sstar(4,6)
bstar(5,1)=sstar(5,6)


cstar(1,1)=sstar(6,1)
cstar(1,2)=sstar(6,2)
cstar(1,3)=sstar(6,3)
cstar(1,4)=sstar(6,4)
cstar(1,5)=sstar(6,5)


dstar(1,1)=sstar(6,6)
```

'Program for assembling system matrix for closed-loop transient control using $\ddot{y}_1$ as controller

'input, first model (continued)"

```
bc=<0;  0;  0;  0;  0;  1/ms>

Gc=<a  bc;  cc  dd>

bd=<0;  -1/m1;  0;  0;  0;  0;  0;  0;  0;  0;  0>

zero(5,6)=0

p=0*ones(11,11)

p(:,2)=<bc*dstar;  bstar>

ident=eye(11,11)

pinv=inv(ident-p)

aprime=pinv*<a  bc*cstar;  zero  astar>

bprime=pinv*bd

celeven=<k1/m2  c1/m2  -1*(k1+k2+ks)/m2  -1*(c1+c2+cs)/m2  ks/m2  cs/m2  0  0  0  0  0>

sff=<aprime  bprime;  celeven  0>
```

II. Control Using Acceleration of m_1 as Controller Input (Second Model)

The model presented in the previous section utilized a transfer function relating the control force, F_c, to the acceleration of m_1 $(\ddot{y}_1)$, that was solved for indirectly. Though not presented here, direct application of Snowdon's Four Pole Analysis (1968, 1979) yields a lower-order transfer function relating these two parameters. This function is:

$$\frac{F_c(s)}{\ddot{y}_1(s)} = \frac{(m_sc_1)s^3 + (c_1c_s + k_1m_s)s^2 + (k_1c_s + c_1k_s)s + k_1k_s}{s^2(c_ss + k_s)}$$

which was numerically transformed into a state-space equivalent using MATRIX$_x$:

$$[\dot{w}] = [A^{**}] \quad [w] + [B^{**}] \quad [\ddot{y}_1]$$

$$[F_c] = [C^{**}] \quad [w] + [D^{**}] \quad [\ddot{y}_1]$$

where:

$$[A^{**}] = \begin{bmatrix} 0 & 1.0 & 0 \\ 0 & 0 & 1.0 \\ 0 & 0 & -872.9 \end{bmatrix} \qquad [B^{**}] = \begin{bmatrix} 0 \\ 0 \\ 4096.0 \end{bmatrix}$$

$$[C^{**}] = \begin{bmatrix} 6734.6 & 24.8 & -0.2 \end{bmatrix} \qquad [D^{**}] = \begin{bmatrix} 0.2 \end{bmatrix}$$

16

Now, similar to the last section:

$$
\begin{bmatrix} \dot{x} \\ \dot{w} \end{bmatrix} = \begin{bmatrix} A & B_cC^{**} \\ 0 & A^{**} \end{bmatrix} \begin{bmatrix} x \\ w \end{bmatrix} + \begin{bmatrix} B_cD^{**} \\ B^{**} \end{bmatrix} [\dot{x}_2] + [B_d] \quad [F_d]
$$

$$
\Rightarrow \begin{bmatrix} \dot{x} \\ \dot{w} \end{bmatrix} - \begin{bmatrix} B_cD^{**} \\ B^{**} \end{bmatrix} [\dot{x}_2] = \begin{bmatrix} A & B_cC^{**} \\ 0 & A^{**} \end{bmatrix} \begin{bmatrix} x \\ w \end{bmatrix} + [B_d] \quad [F_d]
$$

and resizing the matrices on the left hand side:

$$
\begin{bmatrix} \dot{x} \\ \dot{w} \end{bmatrix} = [I]_{9x9} \begin{bmatrix} \dot{x} \\ \dot{w} \end{bmatrix}
$$

and:

$$
[P_{NEW}] \equiv \begin{bmatrix} [0]_{6x1} & B_cD^{**} & [0]_{6x7} \\ [0]_{3x1} & B^{**} & [0]_{3x7} \end{bmatrix}
$$

yields:

$$
[I-P_{NEW}] \begin{bmatrix} \dot{x} \\ \dot{w} \end{bmatrix} = \begin{bmatrix} A & B_cC^{**} \\ 0 & A^{**} \end{bmatrix} \begin{bmatrix} x \\ w \end{bmatrix} + [B_d] \quad [F_d]
$$

17

$$\Rightarrow \begin{bmatrix} \dot{x} \\ \\ \dot{w} \end{bmatrix} = [I-P_{NEW}]^{-1} \begin{bmatrix} A & B_cC^{**} \\ \\ 0 & A^{**} \end{bmatrix} \begin{bmatrix} x \\ \\ w \end{bmatrix} + [I-P_{NEW}]^{-1} \; [B_d] \; [F_d]$$

and the output matrix is

$$[C_{NINE}]_{1x9} = \begin{bmatrix} C & [0]_{1x3} \end{bmatrix}$$

where $[C]$ has been previously defined.

Using this model, in the form of the program listing on the following pages, various time-domain and frequency-domain plots were created and are shown in the main body of this paper.

'Program for assembling system matrix for closed-loop transient control using $\ddot{y}_1$ as controller
'input (second model)"

m1=1.25
m2=1.25
ms=2.09
k1=31600
k2=31600
ks=74200
c1=80
c2=80
cs=85

a=<0 1 0 0 0 0;
     -1*k1/m1 -1*c1/m1 k1/m1 c1/m1 0 0;
     0 0 0 1 0 0;
     k1/m2 c1/m2 -1*(k1+k2+ks)/m2 -1*(c1+c2+cs)/m2 ks/m2 cs/m2;
     0 0 0 0 0 1;
     0 0 ks/ms cs/ms -1*ks/ms -1*cs/ms>

bb=<0; -1/m1; 0; 0; 0; 0>

cc=<k1/m2 c1/m2 -1*(k1+k2+ks)/m2 -1*(c1+c2+cs)/m2 ks/m2 cs/m2>

dd=<0>

num=<-1/ms*c1 -1*c1*cs-k1*ms -1*k1*cs-c1*ks -1*k1*ks>
den=<cs ks 0 0>

snew=sform(num, den)

'Program for assembling system matrix for closed-loop transient control using $\ddot{y}_1$ as controller
'input, second model (continued)"

```
anew(1,1)=snew(1,1)          anew(2,1)=snew(2,1)
anew(1,2)=snew(1,2)          anew(2,2)=snew(2,2)
anew(1,3)=snew(1,3)          anew(2,3)=snew(2,3)

anew(3,1)=snew(3,1)
anew(3,2)=snew(3,2)
anew(3,3)=snew(3,3)

bnew(1,1)=snew(1,4)
bnew(2,1)=snew(2,4)
bnew(3,1)=snew(3,4)

cnew(1,1)=snew(4,1)
cnew(1,2)=snew(4,2)
cnew(1,3)=snew(4,3)

dnew(1,1)=snew(4,4)

bc=<0;  0;  0;  0;  0;  1/ms>

bd=<0;  -1/m1;  0;  0;  0;  0;  0;  0;  0;>

zero(3,6)=0

pnew=0*ones(11,11)

pnew(:,2)=<bc*dnew;  bnew>

ident=eye(9,9)

pnewinv=inv(ident-pnew)
```

'Program for assembling system matrix for closed-loop transient control using $\ddot{y}_1$ as controller
'input, second model (continued)"

aprime=pnewinv*<a bc*cnew; zero anew>

.

bprime=pnewinv*bd

cnine=<k1/m2 c1/m2 -1*(k1+k2+ks)/m2 -1*(c1+c2+cs)/m2 ks/m2 cs/m2 0 0 0>

sff=<aprime bprime; cnine 0>